TAMPEREEN TEKNILLINEN YLIOPISTO
TAMPERE UNIVERSITY OF TECHNOLOGY

MARIA PULLINEN

SOLAR CELL POLYMERS AND THEIR MODELING

Master of Science thesis

Examiner: Docent, University lecturer Terttu Hukka
Examiner and topic approved by the Faculty of Natural Sciences on 8th August 2018

ABSTRACT

MARIA PULLINEN: Solar Cell Polymers and their Modeling
Tampere University of Technology
Master of Science Thesis, 55 pages, 13 Appendix pages
November 2018
Master's Degree Programme in Science and Engineering
Major: Chemistry
Examiner: Docent, University lecturer Terttu Hukka

Keywords: PDTB-EF-T, donor polymer, photovoltaic properties, polymer solar cell

Polymer solar cells (PSC) have become a considerable competitor to traditional silicon-based inorganic solar cells. PSCs are in a great interest due to their light-weight, flexibility and low-cost fabrication techniques. The ongoing research pursues a great deal of effort to develop more effective materials in the active layer of a solar cell. The active layer consists of a donor and an acceptor that together participate in transforming light energy into electrical energy. Nowadays, the most interesting donors are polymers that pair up with non-fullerene acceptors in the active layer of a PSC.

A derivative of benzodithiophene, PDTB-EF-T, as a donor and a small-molecule as an acceptor in the active layer of a PSC gave one of the highest power conversion efficiencies so far, as much as 14.2%. The goal of this thesis was to examine the less thoroughly examined photovoltaic properties of the donor polymer PDTB-EF-T with computational calculations. The properties of the polymer studied in this work were the geometry, the electronic structure, the charge-transport properties and the excited states. These characteristics are often studied for the π-conjugated systems of the donor and acceptor materials in PSCs.

The thesis being the first theoretical study of PDTB-EF-T gives new information on the properties of the polymer. New information of the localization of the electronic density and the delocalization of the molecular orbitals of the periodical model that was illustrated with pictures, was provided. The thesis created a great base of the future studies that focus on the electron transport properties and the theoretical studies of the coupling of this donor molecule and the small-molecule acceptor.

The results of the calculations followed the known theories. As the backbone chain length of the model of the polymer increases, the highest occupied molecular orbital (HOMO) and the lowest unoccupied molecular orbital (LUMO) get closer to each other, and thus, the HOMO–LUMO gap narrows. In addition, the increasing backbone chain length decreases the bond length alternation (BLA) values. The planarity of the radical cation resulted proper charge-carrier transport properties. As for the calculations of the excited states, the vertical transitions of the first two singlet and the first triplet excited state of the trimer of PDTB-EF-T correspond to the visible and near-infrared wavelengths.

TIIVISTELMÄ

MARIA PULLINEN: Aurinkokennojen polymeerit ja niiden mallintaminen
Tampereen teknillinen yliopisto
Diplomityö, 55 sivua, 13 liitesivua
Marraskuu 2018
Teknis-luonnontieteellinen diplomi-insinöörin tutkinto-ohjelma
Pääaine: Kemia
Tarkastaja: Dosentti, Yliopistonlehtori Terttu Hukka

Avainsanat: PDTB-EF-T, donoripolymeeri, fotosähköiset ominaisuudet, polymeeriaurinkokenno

Polymeeriaurinkokennoista on tullut varteenotettava kilpailija perinteisille piipohjaisille epäorgaanisille aurinkokennoille. Polymeeriaurinkokennoista ollaan kiinnostuneita niiden keveyden, joustavuuden ja edullisten valmistustekniikoiden vuoksi. Jatkuva tutkimus pyrkii kehittämään tehokkaampia materiaaleja aurinkokennon aktiiviseen kerrokseen. Aktiivinen kerros koostuu donorista ja akseptorista, jotka yhdessä osallistuvat valoenergian muuttamiseen sähköenergiaksi. Nykyään kiinnostavimmat donorit ovat polymeerejä, joiden parina ovat ei-fullereeniakseptorit polymeeriaurinkokennon aktiivisessa kerroksessa.

Bentsoditiofeenin johdannainen, donori PDTB-EF-T, ja pienimolekyylinen akseptori aktiivisessa kerroksessa tuottivat tähän mennessä yhden suurimmista polymeeriaurinkokennon tehonmuuntosuhteista, jopa 14,2 %. Tämän työn tavoite oli tutkia donoripolymeeri PDTB-EF-T:n fotosähköisiä ominaisuuksia laskennallisin menetelmin, mitä ei ole vielä perinpohjaisesti tehty. Työssä tutkitut polymeerin ominaisuudet olivat geometria, elektroninen rakenne, varauksensiirto-ominaisuudet ja viritystilat. Tällaisia ominaisuuksia tutkitaan usein polymeeriaurinkokennojen donorin ja akseptorin π-konjugoituneille systeemeille.

Tämä ensimmäinen teoreettinen tutkimus PDTB-EF-T:stä antaa uutta informaatiota polymeerin ominaisuuksista. Uutta tietoa saatiin periodisen mallin elektonitiheyden sijainnista ja molekyyliorbitaalien delokalisaatiosta, jota havainnollistettiin kuvissa. Työ loi erinomaisen pohjan jatkotutkimuksille, jotka keskittyvät elektronin siirto-ominaisuuksiin ja tämän donorimolekyylin ja pienen akseptorimolekyylin välisen kytkeytymisen laskennallisiin tutkimuksiin.

Tulokset noudattivat tunnettuja teorioita. Polymeerimallin selkärangan kasvaessa korkein miehitetty molekyyliorbitaali (HOMO) ja matalin miehittämätön molekyyliorbitaali (LUMO) lähenevät, mikä siten kaventaa HOMO–LUMO-väliä. Lisäksi, kasvava selkäranka pienentää sidospituusvaihtelun (BLA) arvoja. Radikaalikationin tasomaisuus aikaansaa hyvät varauksen siirto-ominaisuudet. Virittyneiden tilojen laskut osoittivat, että PDTB-EF-T-trimeerin kahden ensimmäisen singlettiviritystilan ja ensimmäisen triplettiviritystilan vertikaalitransitiot vastaavat näkyvän valon ja lyhytaaltoisen infrapuna-alueen aallonpituuksia.

PREFACE

I started working with this Master of Science thesis in June 2018 at the Laboratory of Chemistry and Bioengineering at Tampere University of Technology. The aim of the study was to research a record material of a polymer solar cell. Computational modeling was completely a new subject for me, so familiarizing myself into the topic demanded huge work effort from me.

I want to thank my supervisor Docent Terttu Hukka for providing me an interesting topic for the thesis and guiding me during the whole process. I also want to thank M.Sc.Tech Tuuva Kastinen for advising and helping me with the calculations. I wish to acknowledge CSC – IT Center for Science, Finland, for computational resources.

Special thanks belong to my parents for supporting me and to my sister, who offered helpful peer support and constructing feedback. I also wish to thank my friends at the university and outside of studies for support and great company. Finally, dear thanks to Olli for endless encouragement and perfect patience.

Tampere, 21.11.2018

Maria Pullinen

TABLE OF CONTENTS

LIST OF FIGURES

LIST OF TABLES

LIST OF ABBREVIATIONS AND SYMBOLS

AEA	Adiabatic electron affinity
AIP	Adiabatic ionization potential
BHJ	Bulk heterojunction
BDT	benzo[1,2-*b*:4,5-*b*']dithiophene
BDTT	bithienyl-benzodithiophene
BLA	Bond length alternation
CSC	Center for Scientific Computing
DFT	Density functional theory
DTBDT	2,4,6,8-tetra(thiophen-2-yl)benzo[1,2-*b*:4,5-*b*']dithiophene
DTBDT-EF	derivative of 2,4,6,8-tetra(thiophen-2-yl)benzo[1,2-*b*:4,5-*b*']dithiophene
EA	Electron affinity
FBTA	Fluorine-substituted benzotriazole
IP	Ionization potential
IT-4F	3,9-bis(2-methylene-((3-(1,1-dicyanomethylene)-6,7-difluoro)-indanone))-5,5,11,11-tetrakis(4-hexylphenyl)-dithieno[2,3-*d*:2',3'-*d*']-s-indaceno[1,2-*b*:5,6-*b*']dithiophene
ITIC	3,9-bis(2-methylene-(3-(1,1-dicyanomethylene)-indanone))-5,5,11,11-tetrakis(4-hexylphenyl)-dithieno[2,3-*d*:2',3'-*d*']-s-indaceno[1,2-b:5,6-b']dithiophene
ITO	Indium tin oxide
J71	Poly[[5,6-difluoro-2-(2-hexyldecyl)-2*H*-benzotriazole-4,7-diyl]-2,5-thiophenediyl[4,8-bis[5-(tripropylsilyl)-2-thienyl]benzo[1,2-*b*:4,5-*b*']dithiophene-2,6-diyl]-2,5-thiophenediyl]
HOMO	Highest occupied molecular orbital
LUMO	Lowest unoccupied molecular orbital
NF	Non-fullerene
OPV	Organic photovoltaic
OSC	Organic solar cell
PCE	Power conversion efficiency
PDINO	Perylene diimide functionalized with amino *N*-oxide
PDTB-EF-T	Polymer derivative of 2,4,6,8-tetra(thiophen-2-yl)benzo[1,2-*b*:4,5-*b*']dithiophene
PEDOT	Poly(3,4-ethylenedioxythiophene)
PFN	Poly[(9,9-bis(3'-(*N,N*-dimethylamino)propyl)-2,7-fluorene)-*alt*-2,7-(9,9-dioctylfluorene)]
PSC	Polymer solar cell
PSS	Poly(styrene-sulfonate)
QM	Quantum mechanics
SMA	Small-molecule acceptor
TDDFT	Time-dependent density functional theory
VEA	Vertical electron affinity
VIP	Vertical ionization potential

A	index
B	eigenvalue
b	scalar value
E_0	ground state energy

$E^-(-)$	Anion electronic configuration at the anion geometry
$E^-(0)$	Anion electronic configuration at the neutral geometry
$E^+(+)$	Cation electronic configuration at the cation geometry
$E^+(0)$	Cation electronic configuration at the neutral geometry
$E^0(-)$	Neutral electronic configuration at the anion geometry
$E^0(+)$	Neural electronic configuration at the cation geometry
$E^0(0)$	Neutral electronic configuration at the neutral geometry
E_{el}	electronic energy
ΔE_{ST}	exchange energy
E_{xc}	electron-electron exchange-correlation energy functional
e	charge of the electron
H	Hamiltonian operator
H_{el}	electronic Hamiltonian operator
$\hbar$	Planck's constant divided by 2π
I	index
j	index
k	index
l	index
m_e	mass of the electron
m_k	mass of nucleus k
n	number of particles
$\mathbf{q}_i$	independent variables of the electronic coordinates
$\mathbf{q}_k$	parameters of the nuclear coordinates
$\mathbf{r}_A$	electron density maximum for nucleus A
r_A	the radial distance from A
r_{ab}	distance between particles a and b
S_0	ground state
S_1	the first singlet excited state
S_2	the second singlet excited state
T_1	the first triplet excited state
T_{ni}	kinetic energy of the non-interacting electrons in ground state
V_N	nuclear-nuclear repulsion energy
V_{ee}	classical electron-electron repulsion potential in ground state
V_{ne}	nuclear-electron interaction potential in ground state
Z	atomic number
∇^2	Laplacian operator
λ	intramolecular reorganization energy
λ^-	intramolecular reorganization energy for electron transport
λ^+	intramolecular reorganization energy for hole transport
λ_1^-	energy needed to reorganize the anion geometry to the neutral state
λ_1^+	energy needed to reorganize the cation geometry to the neutral state
λ_2^-	energy needed to reorganize the vertically ionized neutral state to the anion geometry
λ_2^+	energy needed to reorganize the vertically ionized neutral state to the cation geometry
υ	operator
$\bar{\rho}$	spherically averaged density
Ψ	wave function
Ψ_{el}	electronic wave function

1. INTRODUCTION

The world population growing rapidly makes energy consumption increase. The worry about fossil fuels running out makes developing and manufacturing renewable energy sources important for the use in the future. Organic solar cells (OSC) are expected to have a significant part of energy production due to their clean and inexpensive manufacture, even though they do not yet reach the efficiencies of inorganic solar cells. [1] Moreover, polymer solar cells (PSC) have interested researchers as a renewable and a promising technology, because they are lightweight, mechanically flexible, and they have great potential [2].

Now, the first aim of the PSC investigation is to improve power conversion efficiencies (PCE). The ongoing research in this field focuses on the material design of donor and acceptor molecules that participate in gaining high PCEs in PSCs [2]. Donor and acceptor materials are in the central part of a photovoltaic effect that a solar cell creates. A detailed description of the nature of a molecule used in a PSC is very important, when designing new and more efficient materials. Research in molecular state provides keys to understand, how light energy can be harnessed into electrical energy in the most high-performance way in a PSC. The highest PCE of a PSC so far has been reported to be 14.2% by Li *et al.* [2]. The donor material in the cell was a polymer derivative of 2,4,6,8-tetra(thiophen-2-yl)benzo[1,2-*b*:4,5-*b*']dithiophene (DTBDT), named PDTB-EF-T, and the acceptor material a small-molecule acceptor (SMA) 3,9-bis(2-methylene-((3-(1,1-dicyanomethylene)-6,7-difluoro)-indanone))-5,5,11,11-tetrakis(4-hexylphenyl)-dithieno[2,3-*d*:2',3'-*d*']-s-indaceno[1,2-*b*:5,6-*b*']dithiophene (IT-4F) [2].

The goal of this study was to examine the photovoltaic properties of the donor polymer PDTB-EF-T computationally. The photovoltaic properties of the PDTB-EF-T polymer have not been investigated computationally to the author's knowledge, yet. Only the highest occupied molecular orbital (HOMO) and the lowest unoccupied molecular orbital (LUMO) properties have been studied for the starting structure of PDTB-EF-T, the derivative of DTBDT, named DTBDT-EF, without the side chains. The features of PDTB-EF-T that were studied in this work are the optimized geometry, the electronic structure, the charge-carrier transport properties and the nature of the excited states. The quantum mechanical (QM) methods required for the calculations were applied using Gaussian 16 [3] software. In addition, Avogadro 1.2.0 [4] and Chemcraft 1.8 [5] softwares were used for construction and visualization of the molecules. By examining carefully the photovoltaic properties of this record material, even more efficient molecules can be designed and their performance understood.

The theoretical estimations of the photovoltaic properties in this work are approximations to the experimental value. This study does not consider for example intermolecular interaction or solvent effect. Within the view of different theoretical approaches predicting the properties of a compound can be used to guide the experimental efforts for novel polymer solar cell systems.

This thesis is structured into six chapters. Chapter 2 introduces the basic information of PSCs and some recent development of the active materials. Next, chapter 3 focuses on the QM methods and the molecular scale properties that are used in this thesis. Chapter 4 explains, how the computational calculations were carried out to examine the polymer PDTB-EF-T. The results and discussion are presented in chapter 5. Lastly, chapter 6 summarizes the work by concluding research methods, results and future views.

2. POLYMER SOLAR CELLS

A polymer solar cell is a type of organic photovoltaic (OPV) that can convert light into electricity by the photovoltaic effect [6]. Initially, an organic photovoltaic device was based on donor–acceptor small-molecule single heterojunction that performed a power conversion efficiency of ~1%. During the last decades bulk heterojunction (BHJ) development has been increasing and resulting PCEs of over 10%. In a typical BHJ OPV cell, the photoactive layer is consisted of a conjugated polymer donor and a small-molecule acceptor. There are also all-polymer BHJs, of which both donor and acceptor materials are polymers. [7] This thesis focuses on BHJs that has a polymer donor and a small-molecule acceptor material.

This chapter tells about the basics of polymer solar cells and introduces recent development in PSC materials. The chapter introduces the relevant information of PSCs of this thesis. At first, section 2.1 explains the structure of a polymer solar cell. What kind of polymers and small-molecule acceptors there are in the active layer of a PSC, is described in sections 2.2 and 2.3. Next, section 2.4 explains in detail the working mechanism of a PSC. Section 2.5 focuses on the recent development of materials used in the active layer. Lastly, section 2.6 introduces computational theory that is used in this study.

2.1 Structure of polymer solar cells

An organic solar cell consists of an active material, which includes a p-type conjugated polymer donor and an n-type semiconductor acceptor material, between two electrodes and a substrate to which the system is attached. [6] The substrate does not participate in the photovoltaic effect. It prevents oxygen and water to diffuse into the device and it is often made of glass. On top of the substrate is a transparent electrode. The most common material used as the anode is indium tin oxide (ITO). Another electrode, the cathode, must have a work function lower than that of the anode. The different work functions create an electric field inside the device, which causes collection of electrons at the cathode and collection of holes at the anode. For example, aluminum is used as cathode is PSCs. There are also interfacial layers on both sides of the active layer to prevent holes and electrons' leaking to electrodes. [8] A schematic picture of a PSC can be seen in Figure 2.1.

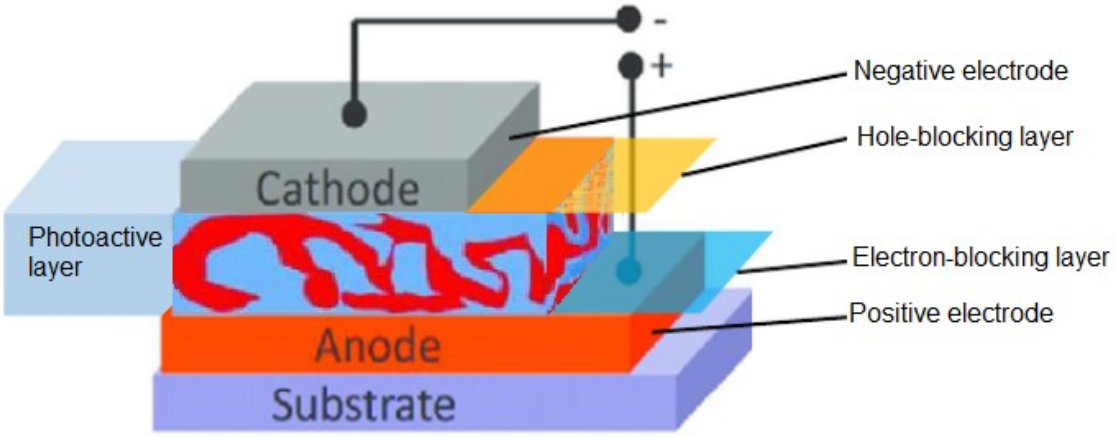

Figure 2.1 *The basic structure of a bulk heterojunction solar cell. Figure modified from reference [9].*

There are different structures of the active material, but the BHJ solar cells are proved to be the most promising way to build an organic solar cell. In a BHJ solar cell, the BHJ layer consists of the donor and the acceptor material that are blended together in organic solvents as an interpenetrating network. This structure increases the interfacial area of the donor and the acceptor materials, which reduces the dissociation distance of the exciton before reaching the interface of the materials. [10] Thus, all excitons are more likely to find an interface and split before the unwanted charge recombination. [6] In bulk heterojunction the interfaces of donor and acceptor materials are spread throughout the whole active layer, which can be seen in Figure 2.1. In addition, the donor and acceptor materials must form a continuous network to the electrodes so that holes and electrons are collected to the contacts [11]. All the polymer solar cell systems examined in this thesis are bulk heterojunction solar cells.

2.2 Polymer donors

There are a few types of the construction ways of donors that can be used in the active layer of a PSC. One option is that the whole polymer consists of one type of a monomer. Another option as a donor polymer is a copolymer, where an electron rich donor and an electron deficient acceptor unit alter [12]. The latter is called a D–A copolymer [12]. Usually, the units consist of five or six membered rings attached to each other to form a planar geometry that contributes to charge transfer. The rings in the polymer backbone form a chain, where single bonds and double bonds alter forming a π-conjugated system. Typical molecules used in donor units are thiophene, bithiophene and benzodithiophene (BDT) and in acceptor units naphthalene diimide, benzothiadiazole, and thienopyrroledione. [13]

The backbones of polymer molecules used in organic solar cells have extended conjugated systems. The p_z-orbitals of the electrons of the hydrocarbons have a delocalized bonding π-orbital and an antibonding π*-orbital. The π-orbital is HOMO and the π* is

LUMO. As for a material, the gap between the valence band and the conduction band is called a band gap and it is typically 1–4 eV. [6] As for a molecule, the gap between HOMO and LUMO is called a HOMO–LUMO gap [14]. An increasing backbone chain length narrows the HOMO–LUMO gap, as one would expect [15]. The HOMO and LUMO levels of a donor should be higher than the corresponding HOMO and LUMO of an acceptor [16]. What should also be kept in mind is that the HOMO level of a donor must be low enough for efficient absorption [17].

Heteroatoms have a great role in organic solar cell materials. It has been found in earlier studies that charge recombination can be prevented with organic materials with high dipole moment [18]. Sulfur atoms in thiophene units, which are often in polymer backbone, have high polarizability that promotes donating electrons and transporting charges [19]. In donors, fluorine atoms are beneficial in benzene units between thiophenes. It has been shown that fluorination contributes to the co-planarity of the polymer backbones and therefore enhances the π–π stacking and charge transport. [20]

Polymers in solar cells have characteristically hydrocarbon side chains. To make a material with decent solubility in a wanted solvent, one must include suitable side chains on the backbone. The most popular side chains tested are alkanes, branched alkanes, alkoxies, ketones, and esters. These kinds of side chains also provide a good influence on the blend morphology of bulk heterojunction. [21] The molecules should cause a minimum degree of steric hindrance, which is gained with less twisted backbone and therefore a more planar structure. [22][23]

Interaction between light and donor materials and thickness of the active layer are very important to consider carefully when designing photovoltaics. The polymer active layer is efficient in collecting photons, if the absorption spectrum of photoactive polymers matches the solar emission spectrum. The layer should also be thick enough to absorb all the photons that reach the polymers. In addition, the electron energy difference between the donor and the acceptor should be bigger than the exciton binding energy, so that the exciton goes through the charge transfer from the donor to the acceptor at their interface. [10]

2.3 Small-molecule acceptors

The acceptors in PSCs can be divided into two parts, the fullerene acceptors and non-fullerene (NF) acceptors [24]. Fullerene-based acceptors have dominated the OSC research for more than two decades [25]. The age of NF acceptors began in the year 2013 including interest in NF SMAs. NF acceptors have already reached better PCEs than the best fullerene-based OSCs [25].

The state-of-the-art NF acceptors can be divided into two categorizes due to their chemical structure: acceptors that have fused aromatic diimides, and acceptors that have strong

intramolecular electron push-pulling effects. These kinds of acceptors have two similar features. First, they have highly electronegative elements in π-conjugated functional groups modified in conjugated backbones that provide strong electron-accepting abilities. The electronegative element can be an oxygen in the form of a carbonyl group, or a nitrogen in the forms of a cyano group or hetero-aromatic segments including a nitrogen. Second, the π-electrons in the functional groups can delocalize into the backbones that guarantees a relatively low reorganization energy. Thus, the accepted electrons can be transported effortlessly without being trapped. [25]

NF acceptors have a great amount of opportunities as solar cell materials. They are in great interest when studying OPVs due to their tunability in absorptivity, optical band gap and frontier molecular orbitals [24]. The synthetic methods, material design and device engineering of fullerene derivatives of OSCs have promoted the development of NF OSCs in recent years. The donor molecules designed for fullerene derivatives are very tunable for NF acceptors, including tuning the absorption spectra and energy levels. In fact, NF acceptors have ability to separate excitons efficiently upon low driving energies, unlike fullerene-based acceptors. Another key advantage of NF OSCs is tuning the absorption spectra and the energetic levels independently. It is a straightforward method to increase the photovoltaic efficiency. [25]

There are also some challenges in NF acceptors as solar cell materials. The anisotropic structure of NF acceptors is a challenge, when it is a matter of the orientation of a donor and an acceptor. The orientation affects the π–π interaction of active materials that is very important for the charge transport. Unlike the isotropic ball-like conjugated backbone in fullerene derivatives, NF-based molecules make it more challenging to guarantee efficient π–π interaction. Thus, it is important to pair a suitable donor with an acceptor of which chemical structures fit to each other and guarantee the right orientation and phase separation. In addition, state-of-the-art SMAs are all amorphous, which sets requirements for polymer donors to form suitable morphology. The amorphous morphology sets drawbacks in charge carrier mobility, because in this case only planar conjugated backbones and high crystallinity are helpful for charge carrier transport properties. [25]

2.4 Operation of polymer solar cells

Polymers work as a photoactive layer in polymer solar cells, because they absorb light and generate and transport charges. A photovoltaic process includes the formation of excitons, which are electron–hole pairs, and the creation of free carriers with incident photons. After the separation of an exciton to individual charges, the free charges migrate through transporting materials and end up in electrodes. [26] This process is illustrated in Figure 2.2. When solar energy is harvested into electrical energy, the process must occur

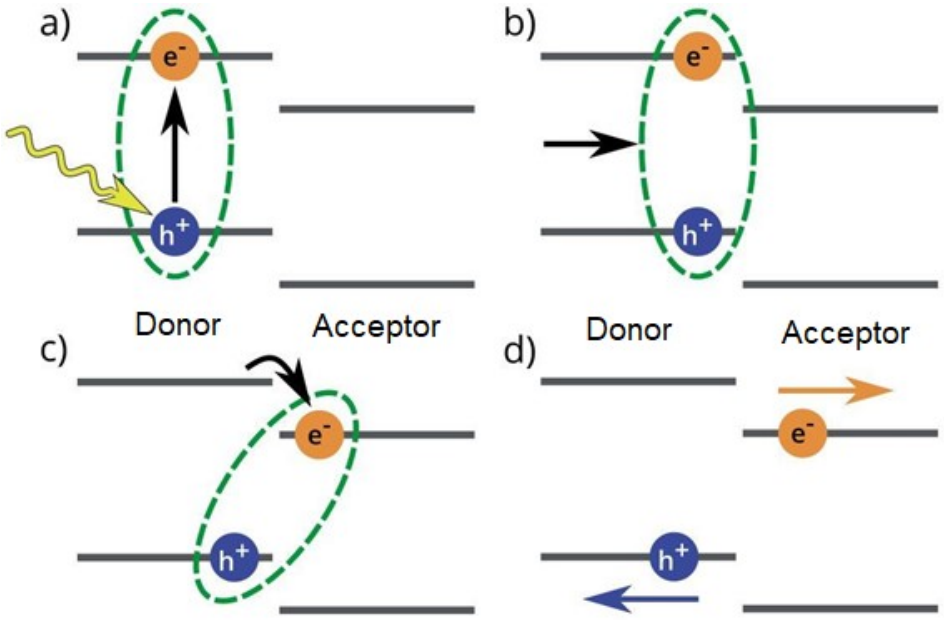

Figure 2.2 *Solar energy harvesting into electrical energy. The lower level of each material stands for HOMO and the upper for LUMO. The phases are a) absorption of light, b) charge transfer, c) the separation of hole and electron, and d) charge transport and collection. Figure modified from reference [27].*

in a specific order, which is the (i) absorption of light, (ii) charge transfer, (iii) the separation of hole and electron, (iv) charge transport and (v) charge collection [10].

More specifically, absorption of light inside the solar cell excites a region of the donor polymer chain, when an electron moves from HOMO to LUMO of a donor. The excitation forms a hole to HOMO of a donor. This process needs the energy of a photon from light. The electron–hole pair is an excited state and therefore named as an exciton. [6] The binding energy of an exciton in organic semiconductors is usually 0.1–1 eV [11].

Next, the exciton starts to diffuse along a donor due to the electric field. If an exciton comes across with an acceptor, the difference between electron affinities leads to the separation of the hole and the electron [10]. In this case, diffusion length is called the length that an exciton travels between generation and charge recombination. Typically, diffusion length in PSCs is 10 nm. The distance from the formation of an exciton to the interface of a donor and an acceptor must be smaller than the diffusion length. Otherwise, an unwanted process called charge recombination occurs and charge collection in electrodes does not happen. [11]

The following step is the breaking of the exciton. Effective fields, which are set up by making a heterojunction between the different materials, cause the separation of the hole and the electron. The electron drops from LUMO of a donor to LUMO of an acceptor [6]. The separated electron and hole are transported to cathode and anode along acceptor and

donor, respectively, because the electrodes with different work functions create an internal field. [10] Finally, the photocurrent is generated due to the charge collection at the electrodes [28].

2.5 The development of the active materials

Most solar energy radiates in the frequencies of visible light and near-infrared region. Therefore, an efficient harvesting of solar energy requires a large overlap in this region for an absorption spectrum of a PSC. [29] An improvement of photocurrent and photovoltage of a solar cell system can be obtained by modifying the energy levels of the orbitals of the molecules. The improvements in the photocurrent can be carried out by optimizing the absorption of the polymer donor in the short wavelength area. This can be done, for example, by shifting the polymer absorption spectrum to higher energies or by adding conjugated side chains to improve the absorption of short wavelength area. A photovoltage increase can be gained by enhancing the energetic offsets between the donor and the acceptor materials, which can be done, for example, by downshifting the energetic levels of the donor and upshifting those of the acceptor. [25]

Another way for better harvesting of the solar spectrum and increasing its efficiency is to use low band gap materials. To improve the photovoltaic performance of polymer:SMA devices, the wide band gap and the deep HOMO level of donor polymers is necessary with SMAs [2]. Controlling band gap is an important issue for research nowadays. Modifying band gap contributes to the electrical and optical properties of the materials and lowering it to approximately to zero is thought to give a conducting material. The method has been to apply alternating donor–acceptor repeating units that have narrow band gaps, [30] which can be seen in a high PCE resulting materials published in the year 2016.

In 2016, one of the highest PCE giving materials tested in organic solar cell was a polymer named poly[[5,6-difluoro-2-(2-hexyldecyl)-2*H*-benzotriazole-4,7-diyl]-2,5-thiophenediyl[4,8-bis[5-(tripropylsilyl)-2-thienyl]benzo[1,2-*b*:4,5-*b*']dithiophene-2,6-diyl]-2,5-thiophenediyl] (J71) as a donor, of which constitutional repeating unit (CRU) is illustrated in Figure 2.3. A small-molecule 3,9-bis(2-methylene-(3-(1,1-dicyanomethylene)-indanone))-5,5,11,11-tetrakis(4-hexylphenyl)-dithieno[2,3-d:2',3'-d']-s-indaceno[1,2-b:5,6-b']dithiophene (ITIC), as seen in Figure 2.4, was used as an acceptor. They gave a PCE of 11.41%. [16] Nowadays, the best performing organic solar cell established gave a PCE of 14.2% [2]. The donor used in this experiment was PDTB-EF-T and the acceptor IT-4F that are shown in Figure 2.5–2.6, respectively.

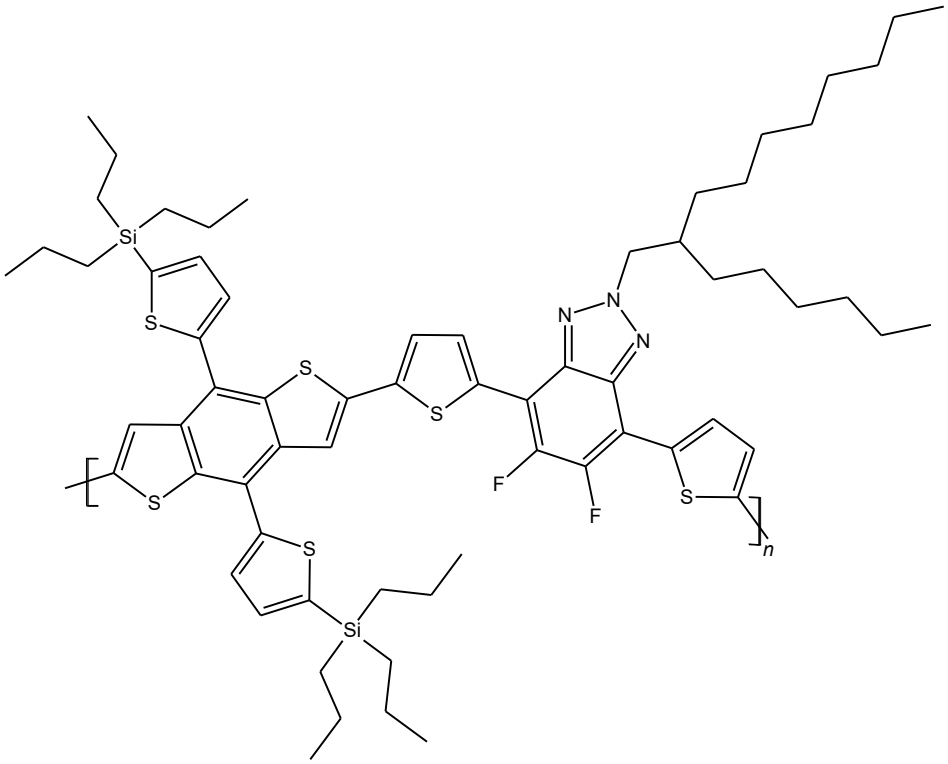

Figure 2.3 *The structure of the constitutional repeating unit of the donor polymer J71, with donor BDTT-Si and acceptor FBTA units. The donor unit, BDTT-Si, contains silicon in this polymer. The other donor unit BDTT-C, does not contain silicon, but carbon.*

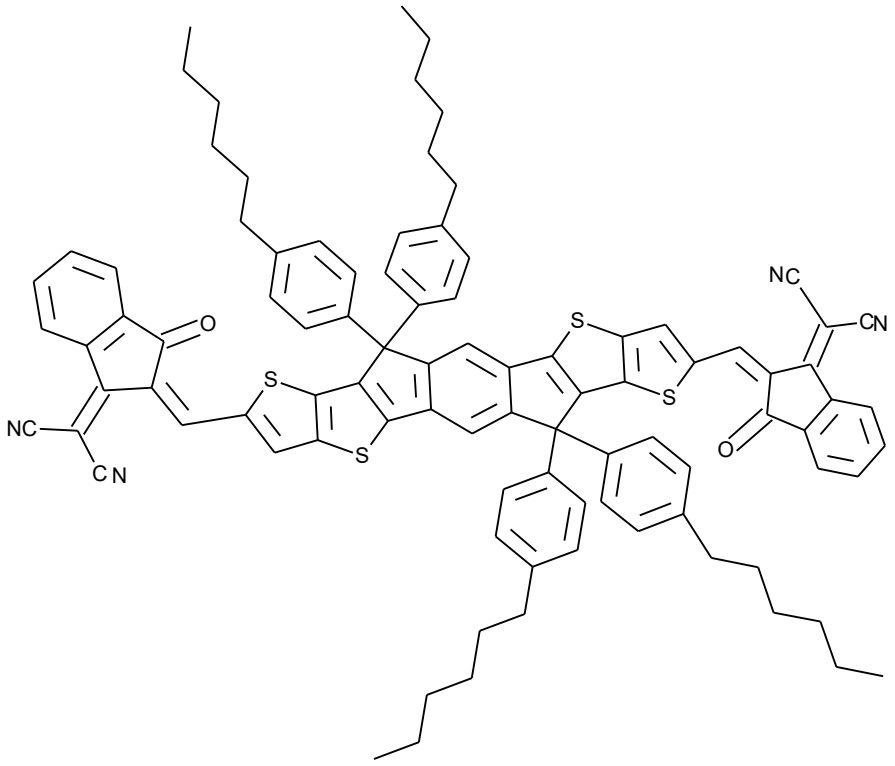

Figure 2.4 *The structure of the small-molecule acceptor ITIC.*

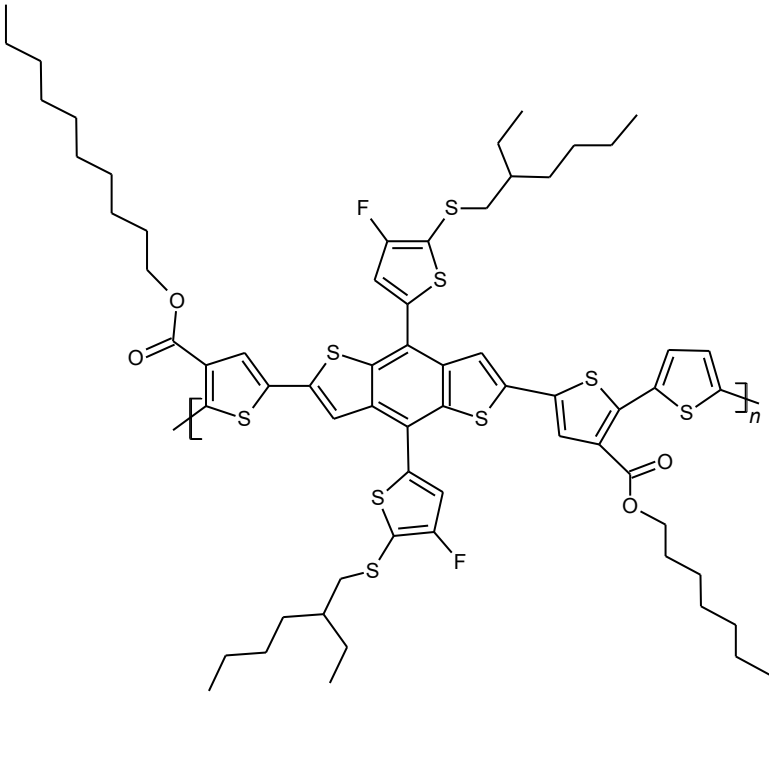

Figure 2.5 *The structure of the constitutional repeating unit of the donor polymer PDTB-EF-T.*

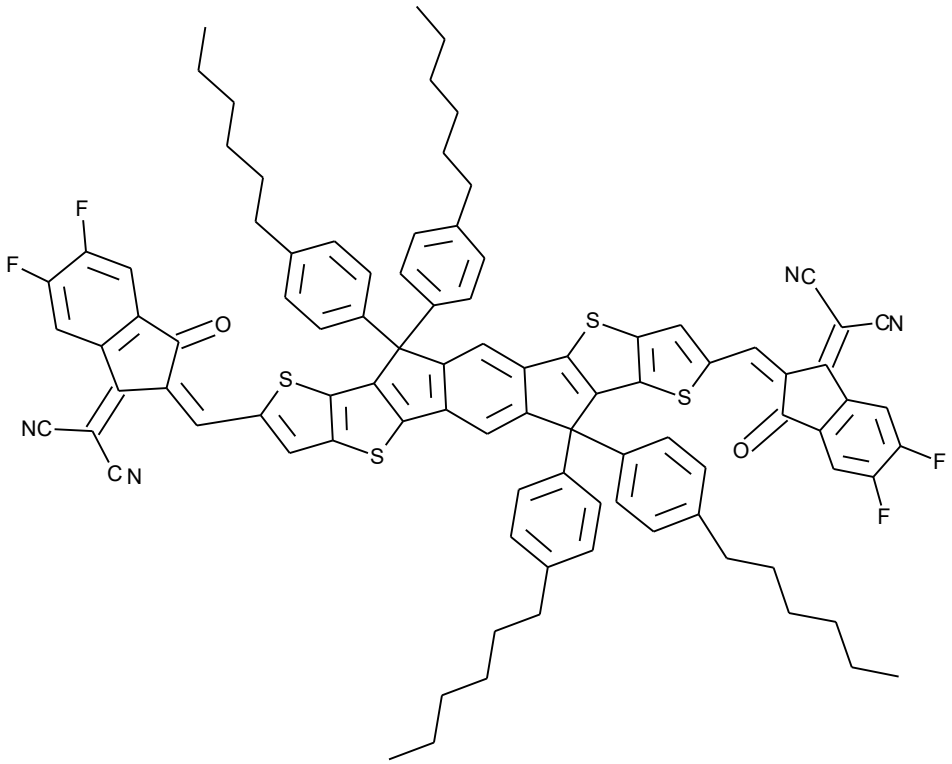

Figure 2.6 *The structure of the small-molecule acceptor IT-4F.*

The following subsections focus on the development, how it is made computationally and experimentally from PCE 11.41% to 14.2%. In subsection 2.5.1, the development of J71

and the experimental details of reaching a PCE of 11.41% are described. The construction of the record material PDTB-EF-T and the experimental details of the PSC of a PCE of 14.2% are explored in subsection 2.5.2.

2.5.1 How ended up in 11.4%

According to an article published in December 2016, a polymer solar cell produced a PCE of 11.41% with a donor material J71 and an acceptor material ITIC. The aim of the study was to increase PCE and decrease the HOMO energy level difference between the donor and acceptor in a D–A copolymer. Both the main chain and the side chain design played an important role when tuning the electronic energy levels and absorption spectra appropriate. The stabilization of the LUMO level and lowering the HOMO level were resulted by the interaction of silicon atoms with aromatic units. The HOMO level of J71 is -5.40 eV and LUMO level -3.24 eV and the band gap 2.16 eV. The silicon atoms also improved crystallinity and hole mobility because of stronger π–π stacking and relatively long C–Si bond. The high crystallinity was also due to a good side chain and fluorine atoms. [16]

The researchers developed D–A copolymers based on bithienyl-benzodithiophene (BDTT) donor unit and fluorine-substituted benzotriazole (FBTA) acceptor unit. The donor unit had different side chains that contained silicon (BDTT-Si) or carbon (BDTT-C). When comparing the donor units BDTT-Si and BDTT-C, the experimentally measured HOMO levels were -5.35 eV and -5.26 eV and LUMO levels -3.40 eV and -3.27 eV, respectively. With density functional theory at the DFT B3LYP/6-31G(d) level with the Gaussian 03 program package, the HOMO levels were -5.17 eV and -5.12 eV and LUMO levels -1.45 eV and -1.33 eV for BDTT-Si and BDTT-C, respectively. The DFT at the B3LYP/6-31G(d) level with the Gaussian 03 was also used to calculate optimized geometry and frontier molecular orbitals of BDTT-Si and BDTT-C. [16]

The device structure of the system was ITO/PEDOT:PSS (poly(3,4-ethylenedioxythiophene):poly(styrene-sulfonate))/J71:ITIC/PDINO (perylene diimide functionalized with amino *N*-oxide)/Al. PDINO was a cathode interlayer to lower the work function of Al. The weight ratio of J71 and ITIC was 1:1 and the thickness of the active layer was about 100 nm. The layers were prepared by spin-coating the 12 mg/cm^3 concentration of the blend solution of J71:ITIC in chloroform at 3000 rpm. A thermal annealing was performed in 150 °C for 10 minutes. [16]

2.5.2 How ended up in 14.2%

According to an article published in May 2018, a polymer solar cell produced a PCE of 14.2% with a donor material PDTB-EF-T and an acceptor material IT-4F. The aim of the study was to enhance the PCE of a polymer and SMA device with the development of DTBDT. When designing low photon energy loss materials, one must achieve a donor molecule with a wide band gap and a deep HOMO level to pair them with SMAs. PDTB-

EF-T gained a low HOMO level of -5.5 eV that is lower than that of J71. The low level is because of the electron-withdrawing fluorine atoms and ester groups in the molecule. Moreover, the modulation of side chains in ester groups contributed to the aggregation effects and molecular packing of the polymer. A linear decyl side chain enhanced organization of the structure and therefore gave highest hole mobility, the most symmetric charge transport and less recombination in comparison with investigated linear octyl- and 3,7-dimethyloctyl side chains. [2]

The record material was constructed knowing that benzo[1,2-*b*:4,5-*b*']dithiophene (BDT)-based polymers have been part of efficient photovoltaic properties in NF PSCs. The π-overlap could be stretched and the coplanarity improved with the addition of thiophene units onto BDT sides and adjacent to BDT, which resulted DTBDT. The HOMO levels of DTBDT-based polymers are quite high because of the electron-donating nature of thiophene units. To lower the levels, the researchers added fluorine atoms on the thiophene side groups and ester on the thiophene units on both sides of DTBDT, which resulted in the polymer DTBDT-EF. Finally, a thiophene unit was set between two DTBDT-EF units to avoid the distortion of the backbone, so the new polymer PDTB-EF-T was created. [2]

It has been calculated by density functional theory (DFT)-based calculations that DTBDT-EF is a polymer with a wide band gap and a low HOMO level of -5.5 eV and LUMO of -2.34 eV. The calculations considered that the fluorine atoms on the thiophene side group and the ester on the thiophene on both sides of the main chain lower the HOMO level of DTBDT. Locating the ester groups on different sides of the backbone makes the polymer PDTB-EF-T have a planar geometry, according to DFT calculations. The theoretical calculation resulted in a HOMO level of -5.16 eV for DTBDT. The calculations were performed using the Gaussian 09 program package based on the DFT method using B3LYP/6-31G (d,p) basis. The alkyl chains were shortened as methyl groups. [2]

The device structure of the studied photovoltaic cell was ITO/PEDOT:PSS/PDTB-EF-T:IT-4F/ poly[(9,9-bis(3'-(*N*,*N*-dimethylamino)propyl)-2,7-fluorene)-*alt*-2,7-(9,9-dioctylfluorene)] (PFN) -Br/Al. The optimal donor/acceptor ratio was 1:1 by weight, and the optimized blend films were made by spin-coating the 18 mg/cm^3 solution in CB/1,8-diiodooctane with 1:0,005 ratio by volume. The thermal annealing was performed in 150 °C for 10 minutes. [2]

2.6 Computational studies

To improve the performance of organic photovoltaic, the design and synthesis of donor and acceptor materials are very important [24]. Identifying the properties of a system at molecular scale with quantum-chemical techniques helps molecular designing. The detailed information of microscopic levels helps to understand, how the organic materials function in macroscopic level in organic photovoltaics. [31] Excluding the theoretical

study of the DTBDT-EF molecule in the article of the development of PDTB-EF-T [2], a systematic theoretical study of the donor polymer PDTB-EF-T has not been reported.

Before examining the photovoltaic properties of the donor molecule, the geometry of the molecule must be optimized with DFT calculations. The construction of the relatively big molecule is done by optimizing the geometry piece by piece. The geometry optimization means finding the configuration that has the lowest energy, and thus, the most stable geometry as possible, which includes the total convergence. The geometry optimization steps of PDTB-EF-T are studied in section 5.1 and the modelled geometries are studied in section 5.2. Within the geometry optimization, the electronic structure is calculated in section 5.3.

The mobility of a charge defines the drift velocity that a charge has under the effect of an electric field. Thus, the mobility is a measure, how fast a charge carrier can travel in a semiconductor. In organic materials, charge transport happens via hopping between localized states. Even though semiconducting polymers own a property of delocalization of charges, the delocalization spreads only in one dimension through the conjugated polymer backbone. The conjugation is sometimes disrupted, resulting a structure that consists of conjugated polymer segments of different lengths. Thus, charges are localized and need to hop to other conjugated parts. [32]

Charge-carrier transport properties of molecules can be investigated with DFT calculations, when a hopping model is expected. The chemical structure and the properties of π-conjugated molecules affect the efficiency of OPVs, because the mobility of electrons and holes define the performance of electronic devices. A charge hopping model describes charge-carrier transport, which is assumed by parameters that are evaluated by DFT calculations. [33] The charge-carrier transport properties of the polymer PDTB-EF-T are examined in section 5.4.

Time-dependent density functional theory (TDDFT) can be used to examine the excited states of π-conjugated systems at the B3LYP/6-31G(d) level of theory. The adapting of the absorption profiles in OPV materials to imitate the solar flux is enabled by tuning the excited-state energies of the materials. TDDFT offers crucial information when studying the nature of the excitations. In this thesis, TDDFT at the level B3LYP/-31G(d) will be used to explore the excited singlet and triplet states of the molecule PDTB-EF-T. The excitation energies affect MO energies, which play an important role in solar cell systems. Donor and acceptor parts of a molecule have a great influence on the excited states. In the study of polymer solar cell materials, the excited-state characteristics is modified using planarization and chemical substitution. [34] The excited state properties in π-conjugated system of PDTB-EF-T are studied in section 5.5.

An atom can have various excited states, for example a singlet excited state and a triplet excited state. A singlet state means an atomic or a molecular state, where all electron spins

are paired [35]. A triplet state means also an atomic or a molecular state, in which two unpaired electrons have parallel spins [36]. The energy difference between the lowest singlet (S_1) and triplet excited state (T_1), in other words the exchange energy (ΔE_{ST}), influences chemical structure. By realizing the effect, it is necessary to form a general view of the intrinsic properties of the singlet and triplet excitations [37]. ΔE_{ST} helps to understand the positioning and crossing between systems of the excited states in a polymer [37]. A small ΔE_{ST} relates to a delocalized state and thus a small exciton binding energy, while a big ΔE_{ST} indicates a localization of the electron–hole pair and thus a high exciton binding energy. A small ΔE_{ST} is desired in OPVs. [37] The singlet and triplet excited states of the polymer PDTB-EF-T are studied in section 5.5.

3. QUANTUM MECHANICS AND MOLECULAR SCALE PROPERTIES

Macroscopic systems are proved by many theories of classical mechanics, but when very small systems are in question, one must use quantum mechanics [38, p. 1]. A basic assumption in QM claim that a microscopic system can be described with a wave function which describes all the physical properties of the system [38, p. 4]. QM was developed to account for the dichotomy that matter has both particle-like and wavelike properties [38, p. 105].

This chapter briefly introduces theories of QM, conformational analysis, and charge-carrier transport. The first sections focus on the wave function and the analysis of conformations and the last section on the charge-carrier transport properties. More specifically, section 3.1 explains, what a Schrödinger equation and the Hamiltonian operator are. Density functional theory is explored in section 3.2. In section 3.3, conformational analysis is presented perfunctorily. The charge-carrier transport properties of the trimer of PDTB-EF-T are introduced in section 3.4 by studying the nature of the optimized structures of the radical anion and the radical cation.

3.1 The Schrödinger equation

A key feature of QM is that a wave function Ψ exists for any system, and that operators, or functions, which work upon Ψ return the detectable properties of the system. This has a mathematical form of

$$\upsilon\Psi = b\Psi \tag{3.1}$$

where υ is an operator and b is a scalar value for a property of the system. This equation can be presented as

$$H\Psi = B\Psi \tag{3.2}$$

where the operator υ in equation 3.1 returns the system energy, B, as an eigenvalue. H is called the Hamiltonian operator and the equation 3.2 is called the Schrödinger equation. [38, p. 106]

The Hamiltonian operator includes five contributions to the total energy in a system: the kinetic energy of the electrons and the nuclei, the attraction of the electrons to the nuclei, and the interelectronic and internuclear repulsions. Other terms are also required in the Hamiltonian in more complicated situations, for example, in the presence of an external electric or magnetic field. The Hamiltonian has a mathematical form of

$$H = -\sum_i \frac{\hbar^2}{2m_e}\nabla_i^2 - \sum_k \frac{\hbar^2}{2m_k}\nabla_k^2 - \sum_i \sum_k \frac{e^2 Z_k}{r_{ik}} + \sum_{i<j} \frac{e^2}{r_{ij}} + \sum_{k<l} \frac{e^2 Z_k Z_l}{r_{kl}} \qquad (3.3)$$

where *i* and *j* run over electrons, *k* and *l* run over nuclei, $\hbar$ is Planck's constant divided by 2π, m_e is the mass of the electron, m_k is the mass of nucleus *k*, ∇^2 is the Laplacian operator, *e* is the charge of the electron, *Z* is an atomic number, and r_{ab} is the distance between particles *a* and *b*. Thus, Ψ is a function of *3n* coordinates where *n* is the number of particles, which makes solving the Schrödinger equation extremely difficult. [38, p. 107]

To make things easier, the Born–Oppenheimer approximation is evoked. The nuclei of molecular systems move much slower than electrons because of the differences in their mass. Thus, it is suitable to compute electronic energies for fixed nuclear positions. It means that the nuclear kinetic energy term and the attractive electron–nuclear potential energy term are zero, and the repulsive nuclear–nuclear potential energy term becomes constant. With these approximations, the electronic Schrödinger equation is

$$(H_{el} + V_N)\Psi_{el}(\mathbf{q}_\mathrm{i}, \mathbf{q}_\mathrm{k}) = E_{el}\Psi_{el}(\mathbf{q}_\mathrm{i}, \mathbf{q}_\mathrm{k}) \qquad (3.4)$$

where 'el' stands for the Born–Oppenheimer approximation, H_{el} includes the first, third, and fourth terms of the Hamiltonian operator in equation (3.3, V_N is the nuclear–nuclear repulsion energy, $\mathbf{q}_\mathrm{i}$ are independent variables of the electronic coordinates, and $\mathbf{q}_\mathrm{k}$ are parameters of the nuclear coordinates. [38, p. 110]

3.2 Density functional theory

The electron density function is based on the electron probability density function. Unlike the wavefunction, the electron density can be measured. It is a function of three variables, (x, y, z), whereas the wavefunction for a molecule with n electrons has 4n variables. [39] The wave function depends on a spin and three spatial coordinates for each electron, making the wave function very complicated [38, p. 249]. Density function, on the other hand, is physically observable and more easily solved.

With a known density, it is possible to determine the Hamiltonian operator, solve the Schrödinger equation, and determine the wave functions and energy eigenvalues. The Hamiltonian operator depends on the total number of electrons and the positions and atomic numbers of the nuclei. Since the total number of electrons affect the energy, the electron density, which integrated over all space gives the total number of electrons, is found useful when defining the Hamiltonian operator. In addition, the nuclei are point charges of which positions correspond to local maxima in the electron density. Moreover, the nuclear atomic numbers are available too from the density, because for every nucleus A to be found at an electron density maximum $\mathbf{r}_A$

$$\left.\frac{\partial \bar{\rho}(r_A)}{\partial r_A}\right|_{r_A=0} = -2Z_A\rho(\mathbf{r_A}) \tag{3.5}$$

where Z is the atomic number of A, r_A is the radial distance from A, and $\bar{\rho}$ is the spherically averaged density. [38, pp. 249–250]

3.2.1 The Hohenberg–Kohn theorems

Earlier DFT models were used in the solid-state physics, and they had little influence on chemistry. DFT became a real quantum chemistry method, when Hohenberg and Kohn proved two theorems in 1964, the Hohenberg–Kohn existence theorem and the Hohenberg–Kohn variational theorem. [38, p. 252] These two theorems are a base on density functional theory [39].

The Hohenberg–Kohn existence theorem says that the electron density function determines the ground-state properties of an atom or a molecule [39]. It is stated previously that there is a dependence of the energy on the density. In the Hohenberg–Kohn theorem, this density is the non-degenerated ground-state density, and it determines the Hamiltonian operator and the wave function. In addition, the ground-state density defines the external potential, which is the way that electrons interact with each other in DFT. [38, pp. 252–254] Furthermore, the Hamiltonian determines not only the ground-state wavefunction but also all excited wave functions [38, p. 254].

The Hohenberg–Kohn variational theorem says that the density of a system obeys a variational principle [38, p. 254]. More specifically, the theorem states that the true electron density gives the lowest possible energy functional for the system. Only if the right functional can be used this theorem is valid. DFT's key is to find suitable functionals, and Hohenberg and Sham proved that a functional of the density must exist. [38, p. 257][39]

3.2.2 The Kohn–Sham method

The final step solving the wave function is the solution of the Schrödinger equation, which is difficult in most cases. The difficulty lies in the electron–electron interaction term in the correct Hamiltonian. A solution was found by Kohn and Sham in 1965. They understood the simplicity of the situation if only the Hamiltonian operator handled a non-interacting system of electrons. They suggested to solve a system of non-interacting electrons that have the same ground-state density as a real electron system. Thus, the ground state energy functional is

$$E_0[\rho(\mathbf{r})] = T_{ni}[\rho(\mathbf{r})] + V_{ne}[\rho(\mathbf{r})] + V_{ee}[\rho(\mathbf{r})] + E_{xc}[\rho(\mathbf{r})] \tag{3.6}$$

where the terms, respectively, refer to the kinetic energy of the non-interacting electrons, the nuclear–electron interaction, the classical electron–electron repulsion and exchange-

correlation energy. The exchange-correlation energy includes the correction to the kinetic energy, which is because of the interacting nature of electrons, and all non-classical corrections to the electron–electron repulsion energy. [38, pp. 255–256] The Schrödinger equation can be solved, if the term E_{xc} as a function of ρ was known [38, p. 257].

In other words, according to the Kohn–Sham approach, from the energy of an idealized system, which does not have interacting electrons, the energy of a system is expressed as a deviation. The Kohn–Sham equations can be derived from the energy equation and taking the Kohn–Sham orbitals into account by minimizing the energy. [39]

3.3 Conformational analysis

Configuration means the three-dimensional organization of atoms in a molecule in space. The rotation of a single bond causing different arrangement in a molecule can be referred as conformations, conformational isomers or conformers. They appear generally, because a single bond can rotate in room temperature. Conformations are not specifically isomers because they cannot be isolated or separated. It is a shape of a molecule. [40]

Conformational analysis examines kinetic and thermodynamic properties of substances that depend on the conformation of the molecules [40]. Computational simulations carry out conformations and weight their properties according to the free energy [38, p. 97]. The bigger the molecule, the more conformations it usually has. In addition, for bigger molecules the key in conformational analysis is to find out the optimal conformation of the molecule from only little information [38, p. 97]. The study areas of conformational analysis are for example energies and populations of different conformational proportions, which conformers are existing, and chemical results of different conformations. [40]

Conformational analysis began in 1874, when Van't Hoff and Le Bell suggested independently a conformation of the valence electrons of a carbon. They proposed that the four electrons are located towards the corners of a tetrahedron, and the nucleus is in the center. This model excited other chemists to examine more complex molecules, including Barton, who presented the basis of modern conformational analysis in 1950. [40]

QM calculations can be used to indicate the interactions that are responsible for the stability of a conformer. Usually, many different spectroscopic techniques are carried out to identify conformational preference, but QM can analyze the stereo electronic interactions in a molecular structure. There are two stages in conformational analysis. At first, one must determine the stable conformations and their populations. Secondly, one must understand the stereo electronic interactions that are responsible for conformation stability. [41]

Conformational analysis for the molecules in PSCs is very important. As discussed earlier, the morphology of the donor and acceptor play a crucial role in charge mobility and therefore in the device performance. Solving the conformation of the polymer PDTB-EF-T is a key factor of this thesis. Through the conformation, the minimum energy of the molecule, the electronic structure, and other qualities that contribute to the efficiency of OPVs, can be examined.

3.4 Charge-carrier transport properties

Charge-carrier transport properties can be studied with ionization potential (IP), electron affinity (EA), and intramolecular reorganization energy (λ). Oxidation and reduction deform the molecular geometry. IP, EA, and λ are studied for hole and electron transport. [33] In this work, the trimer of PDTB-EF-T is used to model the charge-carrier transport properties of the polymer in section 5.4.

IP is often associated with HOMO and hole transport and EA with LUMO and electron transport [42]. IP means the energy that is required for ionization reaction, or the minimum energy required to remove an electron from the top of the valence band to vacuum level. For a polymer in OPV, the IP value indicates the susceptibility or ease to remove electrons from the polymer by an appropriate electron acceptor. EA, on the other hand, means the energy needed to add an electron to LUMO level from the vacuum level. [43]

λ, on the other hand is defined as a deformation that a charge carrier makes. When a hole or an electron is localized on a molecule the extra charge causes a local deformation in the structure. The most striking deformation happens on the molecule and typically in bond length changes. A more reduced deformation happens in the surroundings. Normally, the reorganization energy is separated into intramolecular and intermolecular components that summed up results the total reorganization energy. [44] The intermolecular components are not examined in this thesis. The intramolecular reorganization energy for hole transport (λ^+) is the sum of the energy needed to reorganize the vertically ionized neutral state to the cation geometry (λ_2^+) and the energy needed to reorganize the cation geometry back to the neutral state (λ_1^+). The intramolecular reorganization energy for electron transport (λ^-) is the sum of the energy needed to reorganize the vertically ionized neutral state to the anion geometry (λ_2^-) and the energy needed to reorganize the anion geometry back to the neutral state (λ_1^-). [45] The potential energy curves for neutral, cation, and anion molecule with the previous values are shown in Figure 3.1.

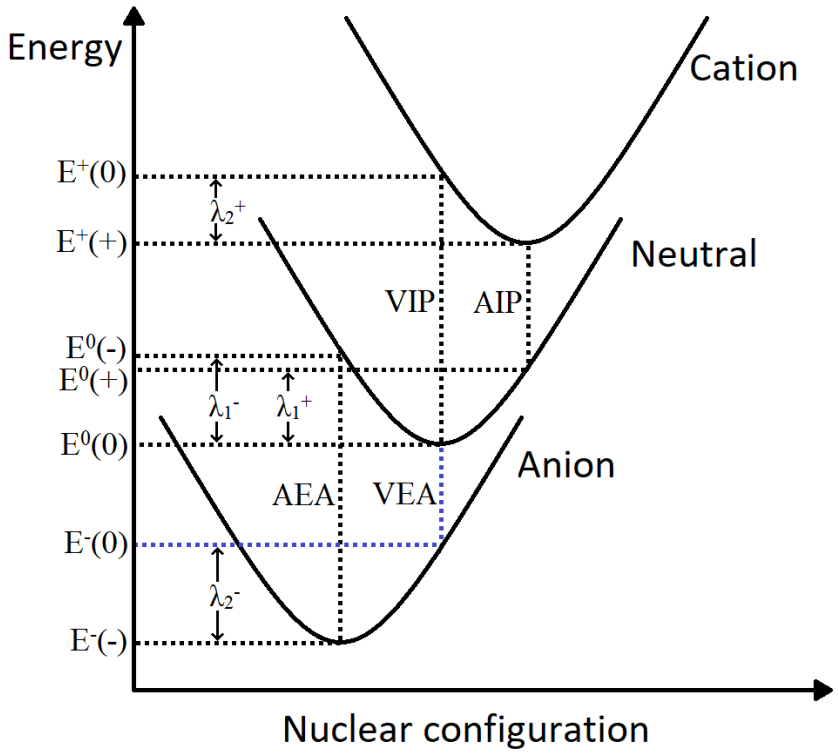

Figure 3.1 *Representation of potential energy curves for neutral, cation, and anion states.*

The IP, EA and λ of the trimer of PDTB-EF-T can be calculated from the energies of the three geometry optimizations, neutral ($E^0(0)$), radical cation ($E^+(+)$), and radical anion ($E^-(-)$) states. The optimized geometries of the radical cation and the radical anion were calculated by starting from the optimized geometry of the neutral molecule. With these optimizations, another four single-point energy calculations that calculate the energy of a geometry without geometry optimization, were performed: the neural electronic configuration at the cation geometry ($E^0(+)$), the neutral electronic configuration at the anion geometry ($E^0(-)$), the cation electronic configuration at the neutral geometry ($E^+(0)$), and the anion electronic configuration at the neutral geometry ($E^-(0)$). These values are used to calculate vertical IP (VIP), adiabatic IP (AIP), vertical EA (VEA), adiabatic EA (AEA), λ_1^+, λ_2^+, λ_1^-, and λ_2^- for the neutral molecule as follows [33]:

$$VIP = E^+(0) - E^0(0) \tag{3.7}$$

$$AIP = E^+(+) - E^0(0) \tag{3.8}$$

$$VEA = E^-(0) - E^0(0) \tag{3.9}$$

$$AEA = E^-(-) - E^0(0) \tag{3.10}$$

$$\lambda_1^+ = E^0(+) - E^0(0) \tag{3.11}$$

$$\lambda_2^+ = E^+(0) - E^+(+) \tag{3.12}$$

$$\lambda_1^- = E^0(-) - E^0(0) \tag{3.13}$$

$$\lambda_2^- = E^-(0) - E^-(-) \tag{3.14}$$

4. MODELS AND METHODS

This chapter focuses on the computational models and methods that were used in this thesis. Section 4.1 explains, how the periodical model was constructed and examined, and section 4.2 focuses on the methods how the calculations were carried out. The results of these modellings and their importance are discussed in chapter 5.

4.1 Models

The CRU of the polymer PDTB-EF-T, which is presented in Figure 2.5 and Figure 4.1 was used to create the monomer, dimer , trimer, and periodic models, as described under section 5.1. The geometry of the monomer was optimized first. Secondly, dimer 1 was constructed and optimized of the two monomer CRUs. The periodic model was calculated from the modified dimer 1 that is the model of dimer 2. Dimer 3 and the trimer were cut from the periodical model and optimized. The trimer was not totally converged. The side chains of each model, except the monomer, were replaced with methyl side chains to make the calculations less demanding. The calculations in sections 5.3 and 5.4 were done with the trimer without the side chains to model the charge-carrier transport properties and the excited state properties to also reduce the computational cost.

The modeling of the polymer was started by optimizing its geometry, in which potential energy surface (PES) scans were necessary. Dihedral angles between atoms were determined with relaxed PES-scans, where the geometry of a molecule was optimized at constrained intervals of 20° between 0° and 360°, except the angle between the two CRUs of dimer 1, of which PES-scan was performed at constrained intervals of 10°. After each PES-scan, the geometries of the molecules were optimized with the coordinates that gave the lowest energy in the PES scan. The geometry optimization ensures the lowest energy.

The basics in examining organic solar cells includes the theoretical knowledge of the HOMO and LUMO energy levels of the molecules. These MO levels of the donor and acceptor materials are crucial features to determine, if an effective charge transfer takes place between the materials. For example, guiding the synthesis of materials with low band gap, quantum-chemical means have been more and more used to predict the band gap of conjugated systems. [30] The MO levels are examined in section 5.3.

Another intrinsic property of a conjugated polymer that gives detailed connections between chemical structure and electronic and optical properties is bond length alternation (BLA). BLA is a geometrical parameter that is calculated as the difference between the lengths of a single bond and a double bond in π-conjugated system. The conjugation path for calculating the BLAs in bold is shown in Figure 4.1. The BLA was calculated for the optimized ground state geometry of the monomer and the periodic model of PDTB-EF-T in the following way in section 5.3: the average difference in length between the adjacent single and double bonds through the conjugation path between the terminal carbons [46].

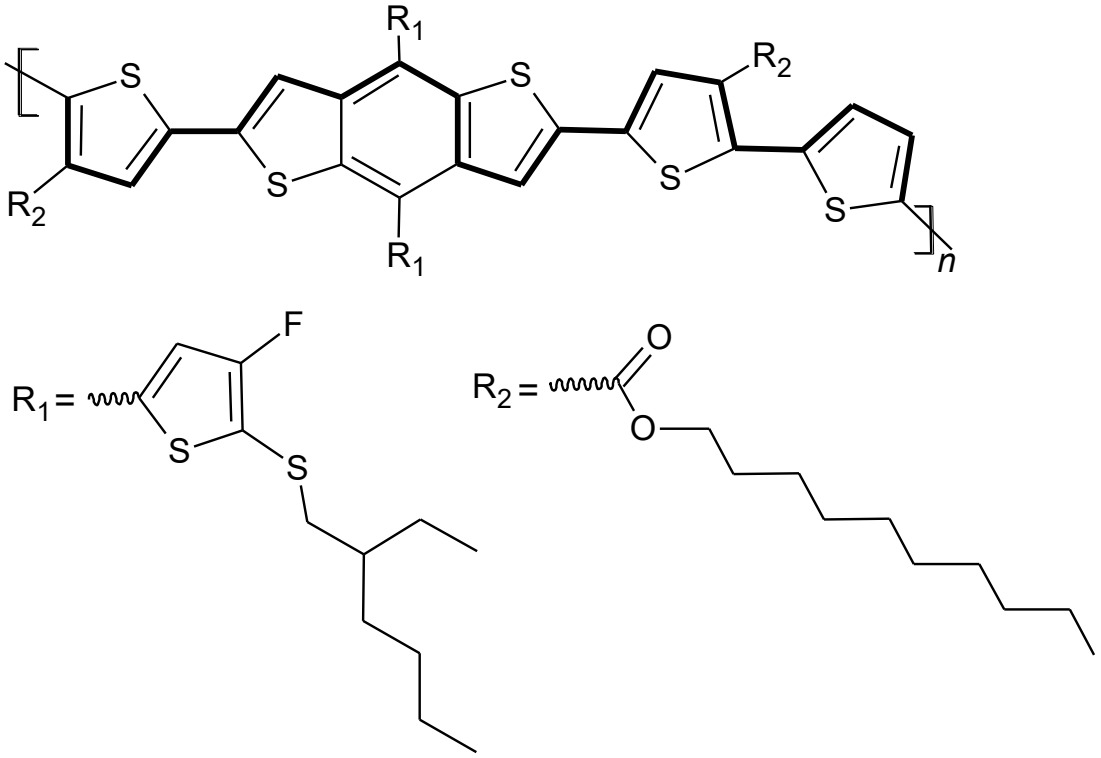

Figure 4.1 *The conjugation path for calculating the BLAs in bold.*

When calculating the BLA of the monomer, dimer 1, trimer, and periodic model, one, two, three, and two CRUs of the molecules were used determining the bond lengths, respectively.

The excited states were calculated for the trimer of PDTB-EF-T using TDDFT at the B3LYP/6-31G(d) level of theory. The trimer was used to model the excited state properties of the PDTB-EF-T polymer, because the TDDFT calculations are not available for the periodic model in Gaussian 16. The geometries of S_1 and T_1 were optimized to examine, how the structure and the electronic behavior of a molecule changes during an excitation. The calculations were started by using the coordinates of the optimized geometry of the ground state (S_0) of the trimer that was calculated in section 5.1. The MOs were calculated for S_1 and T_1 to examine, how excitation influences on the electronic properties. The BLAs were also determined for S_1 and T_1 as the same manner as described earlier to examine, how excitation affects the structural properties of the trimer.

The energies of the vertical electronic transitions for the first ten singlet and triplet excited states were determined for the trimer. The excitations were from $S_0 \rightarrow S_1$, $S_0 \rightarrow S_2$, and so on, and $S_0 \rightarrow T_1$, $S_0 \rightarrow T_2$, and so on. Again, the trimer of PDTB-EF-T was used to model the properties of the polymer. The calculations were started by using the coordinates of the optimized geometry of the ground state. At first, the singlet and triplet excited states were calculated to determine the optical transitions. The results also include information of the excitation energies that determines the electron movement from one MO to another.

With the excited state energies, the exchange energy of the trimer of PDTB-EF-T could be determined in section 5.5.

4.2 Methods

All DFT and TDDFT calculations were carried out in vacuum with Gaussian 16 (Revision A.03) [3] software. The DFT calculations were used for optimizing the geometries of the neutral monomer, neutral dimer 1, neutral dimer 2, neutral dimer 3, neutral trimer and neutral periodic model. The DFT calculations were also used for optimizing the geometries of the radical anion and the radical cation of the trimer. The TDDFT calculations were used for optimizing the geometries of the first singlet and triplet excited states of the trimer. In addition, the TDDFT calculations were used for calculating the energies of the vertical electronic transitions for the first ten singlet and triplet excited states in S_0 geometry. Avogadro 1.2.0 [4] and Chemcraft 1.8 [5] softwares were used for construction and visualization of the molecules.

The geometry optimization calculations and studies of the periodic model were carried out at the B3LYP/6-31G(d,p) level of theory in sections 5.1 and 5.2. The electronic structure of the periodic model in section 5.3 was also examined at the B3LYP/6-31G(d,p) level of theory. In section 5.4, the charge-carrier transport property calculations of the trimer were calculated at the B3LYP/6-31G(d,p) level of theory. The excited state properties of the trimer were calculated at the B3LYP/6-31G(d) level of theory in section 5.5.

5. RESULTS AND DISCUSSION

The results of this thesis consider the modelled properties of the donor polymer PDTB-EF-T. Examining the electronic structure, the charge-transport properties, and the excited states in π-conjugated systems give valuable information about the performance of the materials in polymer solar cells. The methods used in the work to examine the features of the polymer were completely computational. This chapter presents the results and compares them to the experimental research results which have been obtained for the polymer PDTB-EF-T and J71.

The monomer, dimer 1, dimer 2, dimer 3, trimer, and periodic model of PDTB-EF-T were optimized at first. Section 5.1 explains, how the geometry optimization steps for constructing the periodic model were performed. Section 5.2 explores the geometry of the optimized models. Section 5.3 considers the electronic structure of the donor polymer PDTB-EF-T and some properties of the monomer, dimer 1, dimer 2, dimer 3, and trimer. In section 5.4, the results concerning the charge-carrier transport are examined. Finally, the consequences of the excited states and their properties of the polymer are considered in section 5.5. The calculations in sections 5.4 and 5.5 were done with the trimer, because the TDDFT calculations are not available for the periodic model in Gaussian 16.

5.1 Geometry optimization steps for constructing the periodic model

The electronic structure of the polymer PDTB-EF-T was solved by optimizing the molecule piece by piece. To solve the optimized structure of the polymer, the structure of the monomer and dimer 1 were optimized first. At the beginning of the optimization, the backbone of the CRU was optimized one step at a time with hydrogens on the places of the side chains and the next CRU. The calculations were started with the optimization of the structure of BDT that can be seen in Figure 5.1. The second step was to add a thiophene to BDT on its right place and perform an optimization and a PES scan between the sulfurs. The optimized structure of the molecule is shown in Figure 5.2. The previous steps were repeated with the second and the third thiophene units of the backbone shown in Figure 5.3–5.4, respectively.

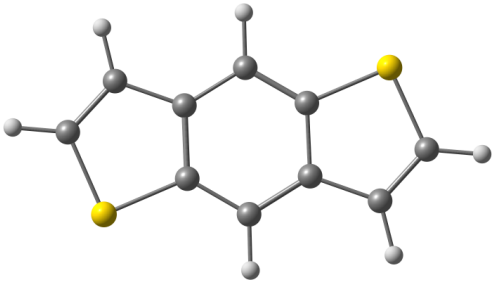

Figure 5.1 *The optimized structure of step 1.*

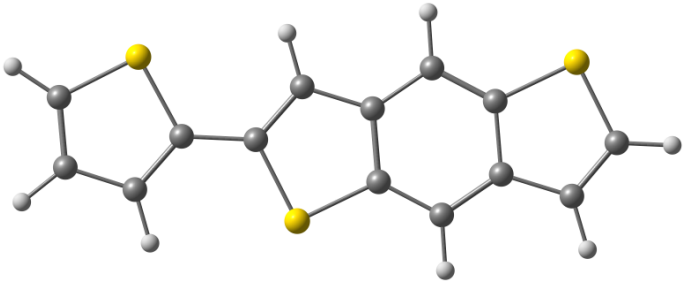

Figure 5.2 *The optimized structure of step 2.*

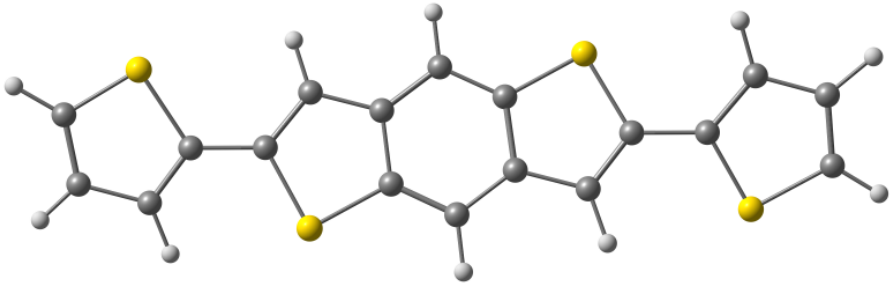

Figure 5.3 *The optimized structure of step3.*

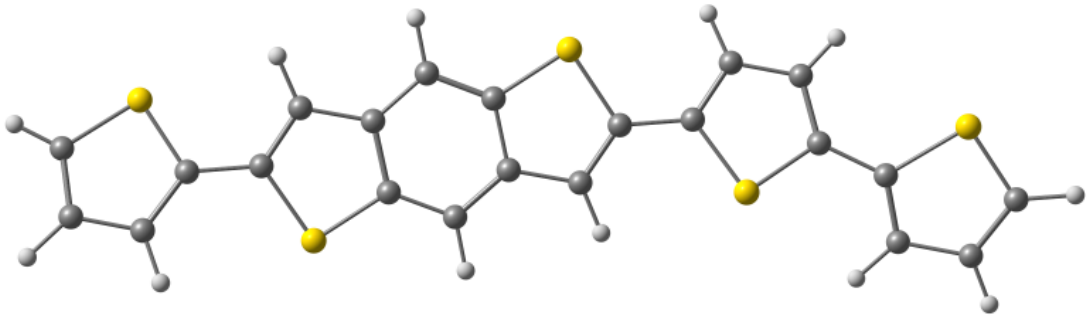

Figure 5.4 *The optimized structure of step 4.*

The fifth step was to add a thiophene unit with a fluorine and an SH-group to the backbone, optimize the structure, perform a PES-scan on it, and optimize the structure again, which can be seen in Figure 5.5. The previous step was performed to the other thiophene unit on the other side of the backbone as well, which is shown in Figure 5.6.

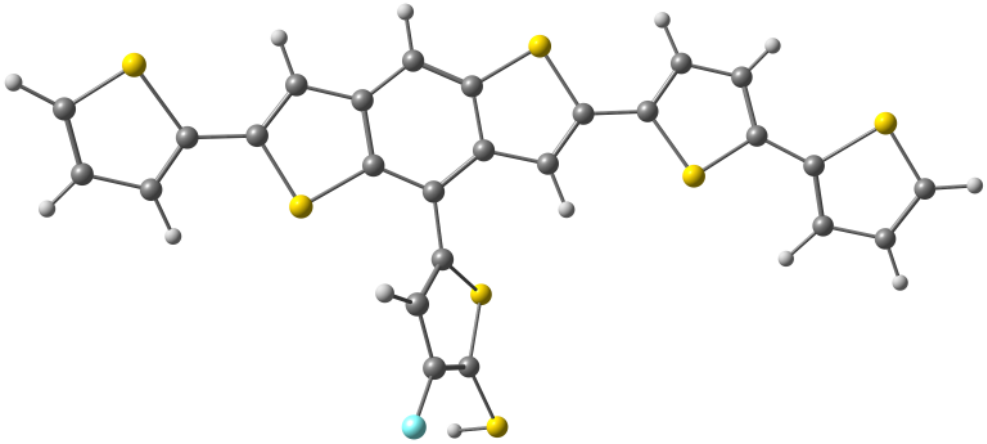

Figure 5.5 *The optimized structure of step 5.*

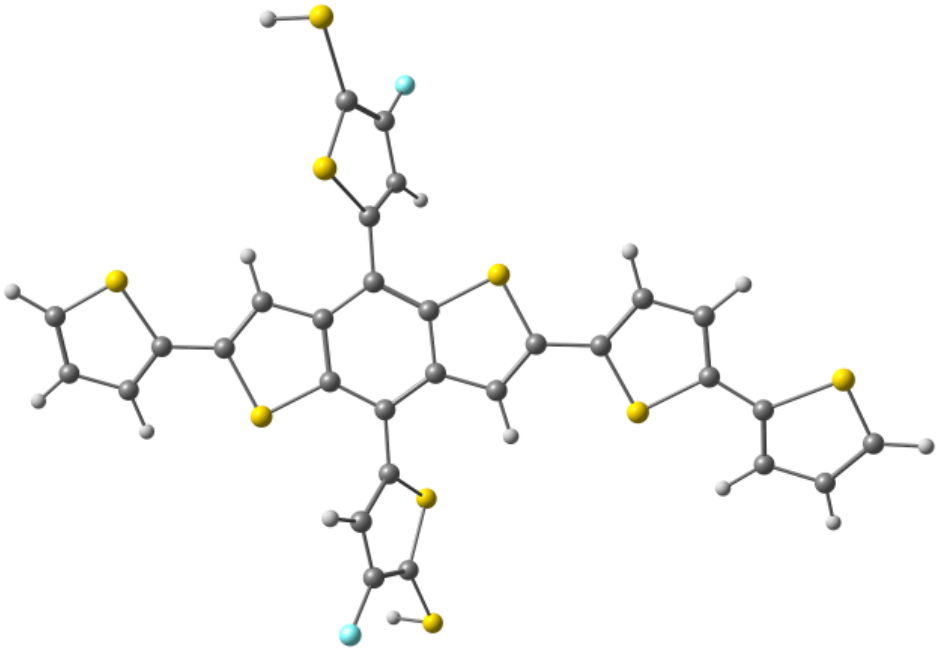

Figure 5.6 *The optimized structure of step 6.*

To continue the optimization of the structure of the polymer PDTB-EF-T in step 7, a carboxyl acid group was added on the place, in which the ester group is located. After the optimization, a PES-scan was performed to know the direction, to which the carboxyl oxygen and hydrogen aim so that the molecule has the smallest energy. Finally, the optimization was performed. The optimized structure is shown in Figure 5.7. The previous step was repeated with the other carboxyl acid group, and the optimized structure can be seen in Figure 5.8.

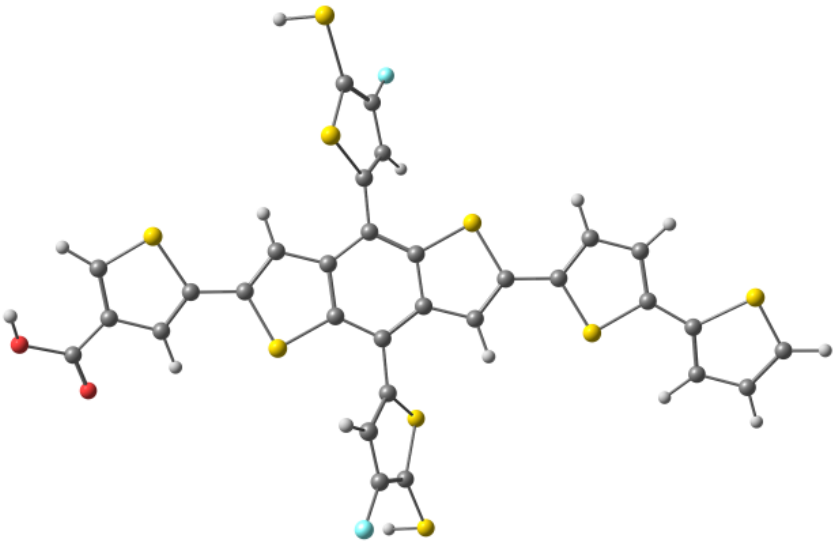

Figure 5.7 *The optimized structure of step 7.*

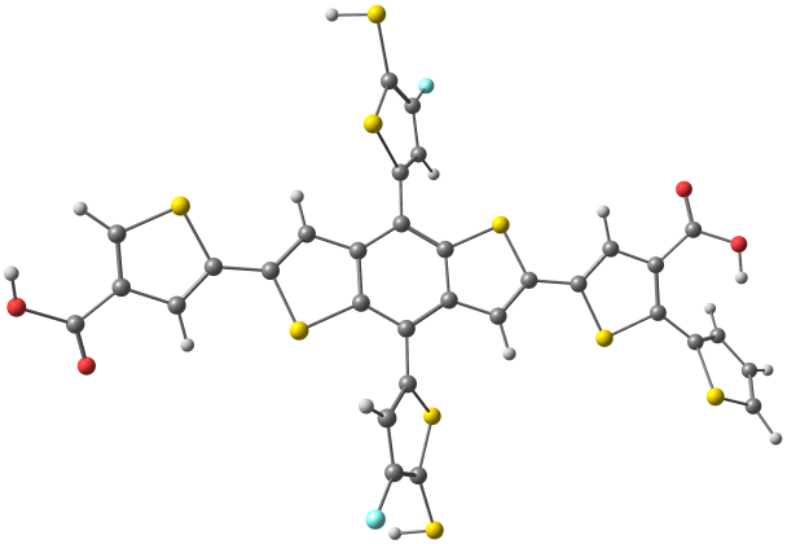

Figure 5.8 *The optimized structure of step 8.*

It can be seen in Figure 5.8 that the hydrogen attached to the sulfur in the upper thiophene unit aims toward the hydrogen in the left carboxyl acid group, which is not a suitable conformation. The problems of this conformation can be predicted, because the side chains of the groups may confront each other. Therefore, another PES-scan was performed for the sulfur–hydrogen bond. The result of the geometry optimization after the PES-scan, in other words, step 9 can be seen in Figure 5.9. The hydrogen of the sulfur has turned in other direction.

It can be noticed that the two sulfurs in the most right are on the same side of the backbone, which may not be the most optimal structure. Thus, another PES-scan and a geometry optimization were performed to the thiophene in the right. It can be seen in Figure 5.10 that the thiophene has not turned and the sulfurs are on the same side of the backbone.

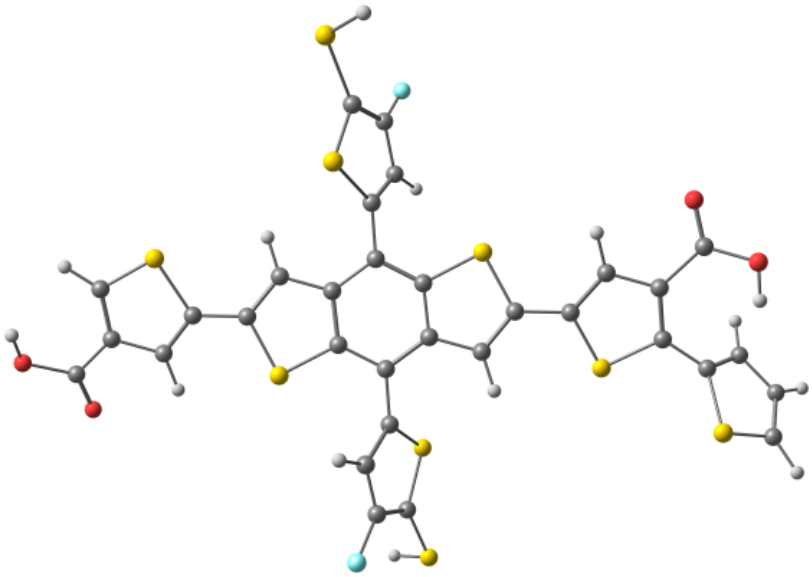

Figure 5.9 *The optimized structure of step 9.*

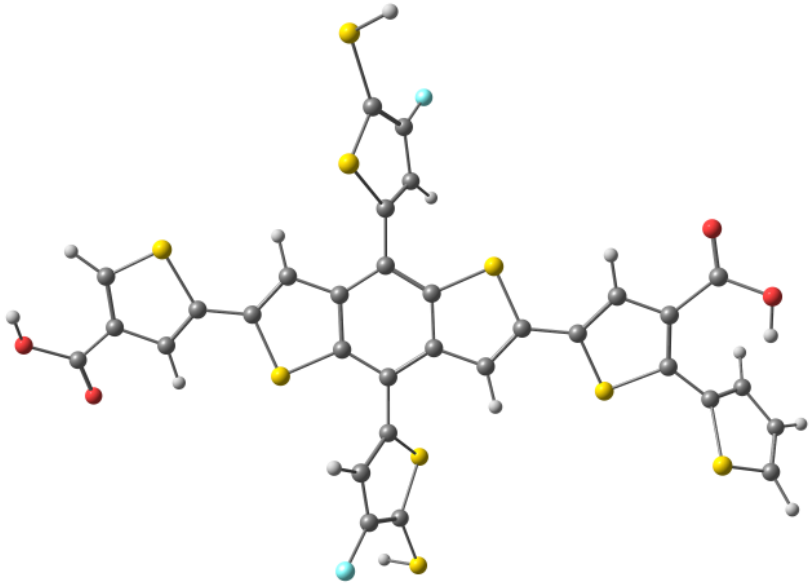

Figure 5.10 *The optimized structure of step 10.*

Finally, the side chains were added to the coordinates of the optimized molecule of step 9, as steps 11 and 12. At first, the geometries of the side chains were optimized. Then, the side chains of the thiophenes were set on the places of the hydrogens. The optimized structure can be seen in Figure 5.11. As step 12, the decyl side chain were added to replace the hydrogens of the carboxyl acid groups, which created two esters. Figure 5.12 visualizes step 12 and is the optimized structure of the monomer of PDTB-EF-T. The exact coordinates, bond lengths, and bond angles of the monomer can be seen in appendices A, C, and D. The labelled atoms are shown in appendix B, in Figures B1–B6.

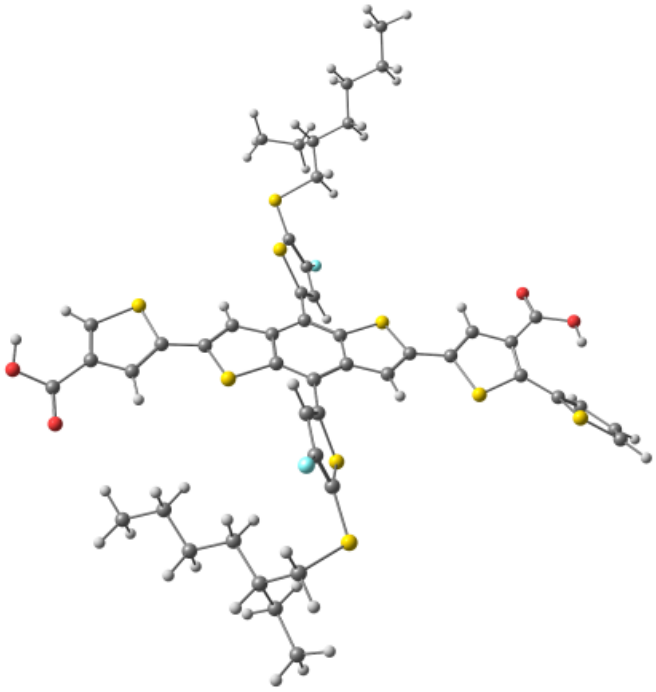

Figure 5.11 *The optimized structure of step 11.*

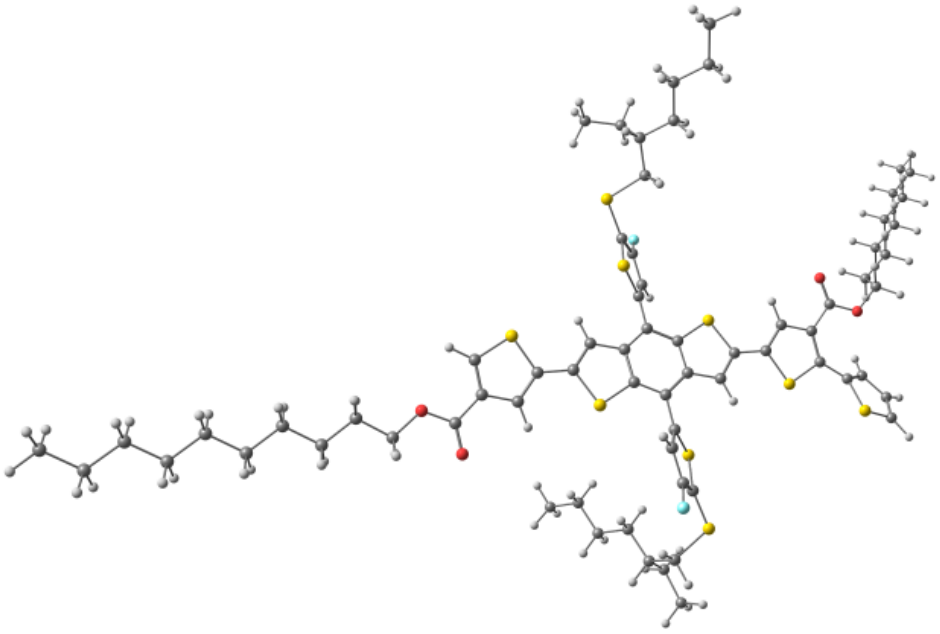

Figure 5.12 *The optimized structure of step 12.*

To begin the optimization of the polymer, the side chains of the monomer were replaced with methyl groups, and the structure was optimized, which can be seen in Figure 5.13. The decyl and the 2-ethylhexyl side chains were simplified as methyl groups, so that the calculations would be computationally less demanding. A dimer with methyl side chains was constructed of the two simplified monomer units. The structure was optimized. A PES-scan was also performed between the two CRUs of dimer 1, and the geometry with the lowest energy was optimized again. The optimized structure is shown in Figure 5.14.

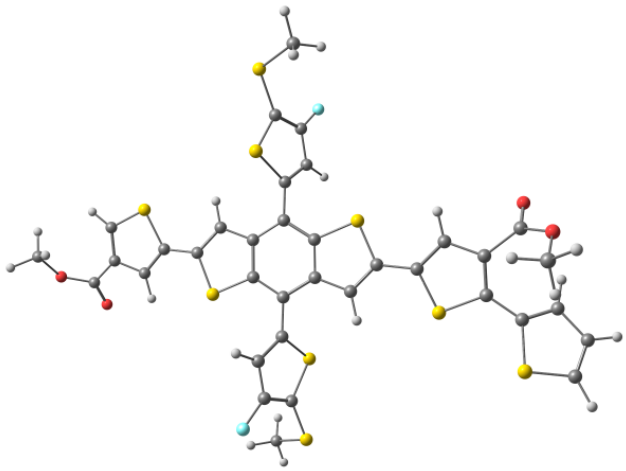

Figure 5.13 *The monomer with methyl side chains.*

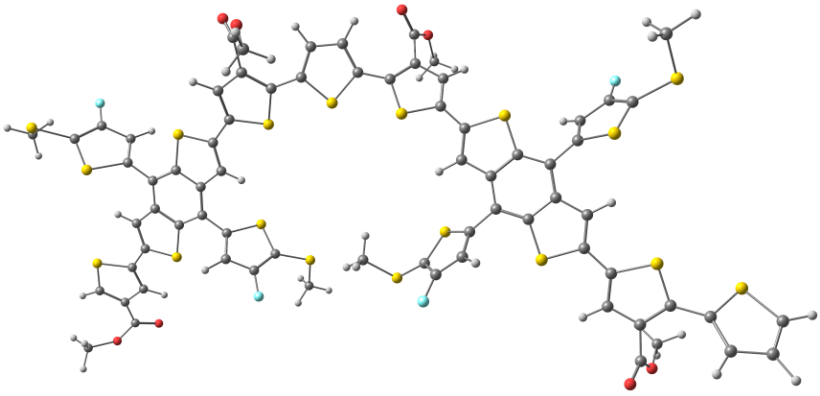

Figure 5.14 *The optimized structure of dimer 1 after a PES-scan and a geometry optimization with methyl side chains.*

Eventually, the periodical calculations were performed from dimer 1. Periodical calculations create the polymeric structure. The structure of the first six CRUs of the polymer PDTB-EF-T is shown in Figure 5.15.

The periodical model was created from dimer 1 model, which does not necessarily calculate the optimized geometry with the minimized energy. Thus, it must be inspected, how the periodical model starts from dimer 1. In Figure 5.16, the bond between the second and the third CRU is shown zoomed. The sulfurs are not in the same side of the backbone and the joint is not like that of the first and the second CRU. Thus, dimer 1 in Figure 5.14 was modified by changing the position of the thiophene and its side chain on the most left. The modified geometry, dimer 2, can be seen in Figure 5.17. Another periodical model that is shown in Figure 5.18 was calculated from dimer 2. The energy of dimer 2 with added hydrogens was calculated with single point energy calculation. Now that the sulfurs are on the same side of the backbone that is planar, and the joints are uniform, the energy is smaller than the periodical model in Figure 5.15.

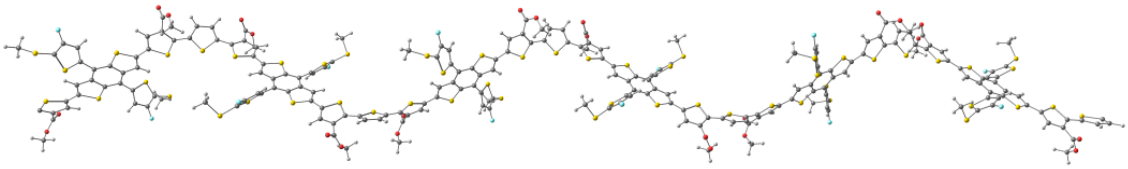

Figure 5.15 *The optimized geometry of the polymeric structure of PDTB-EF-T.*

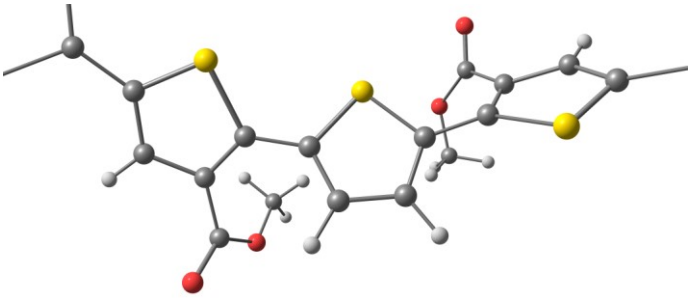

Figure 5.16 *The bond between the second and the third constitutional repeating units.*

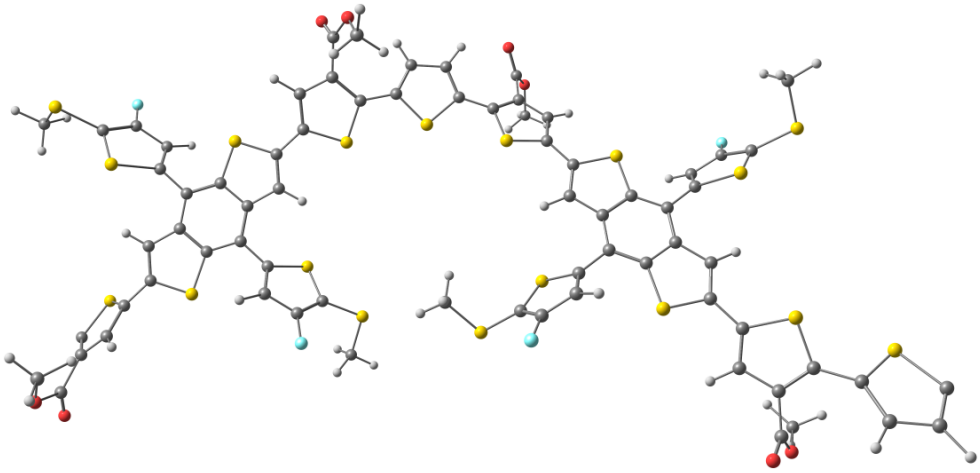

Figure 5.17 *The modified geometry of dimer 1, dimer 2.*

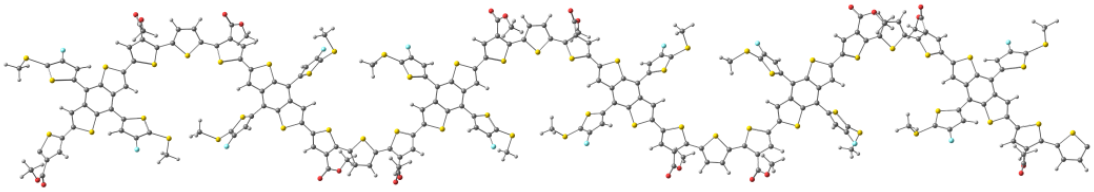

Figure 5.18 *The periodical model calculated from the modifed dimer 1.*

Another dimer, dimer 3 that is shown in Figure 5.19, was constructed by cutting two CRUs from the periodical model. In addition, the geometry of the trimer was optimized. The trimer was constructed from the periodical model by taking three CRUs and adding hydrogens. PES-scans were not performed for the molecule. The optimized structure of the trimer is shown in Figure 5.20.

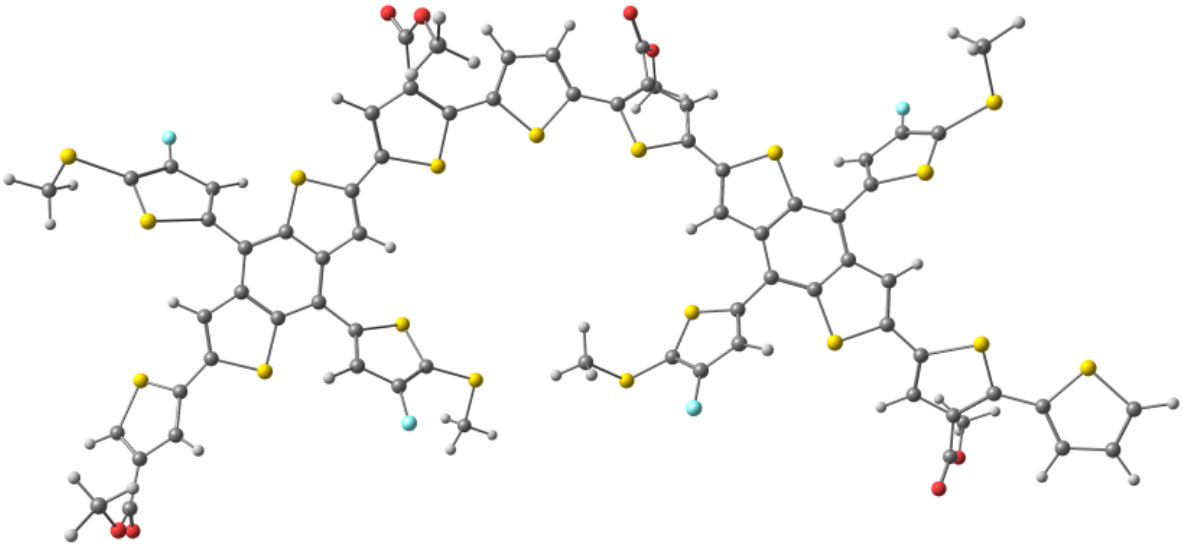

Figure 5.19 *Dimer 3 cut from the periodical model.*

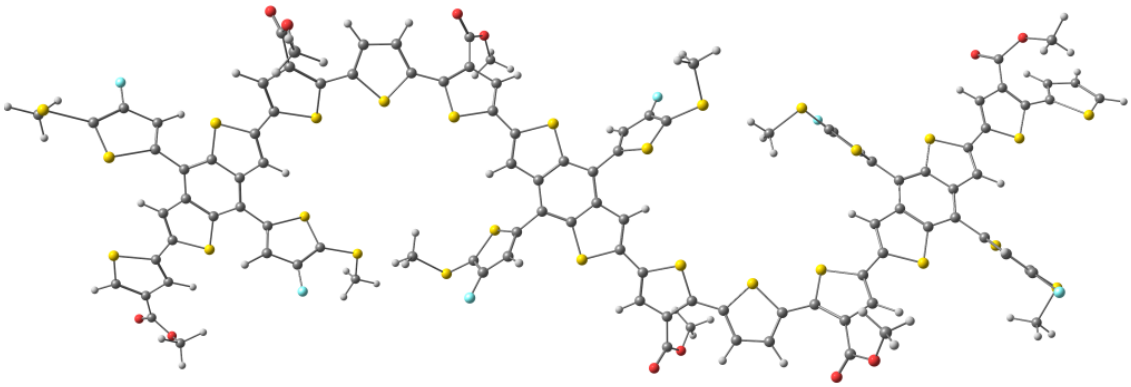

Figure 5.20 *The optimized structure of the trimer.*

5.2 Geometries of the optimized models

The chemical structure of the dimer in the article is shown in Figure 5.21 and that of this work in Figure 5.22. By comparing the structures, the backbone can be seen to be different. Results are affected by the choice of the CRU.

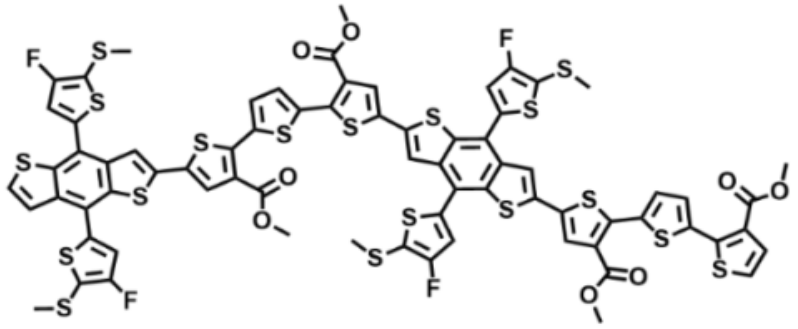

Figure 5.21 *The dimer as presented in the article. Modified from reference [2].*

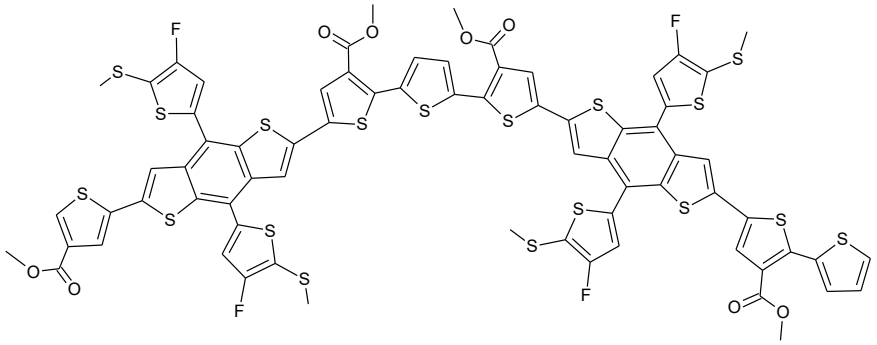

Figure 5.22 *The dimer modelled in this work.*

The monomers, the oligomers, and the periodical model of PDTB-EF-T were optimized with Gaussian 16 [3] at the B3LYP/6-31G(d,p) level of theory. It can be seen in Figure 5.13 that the backbone of the monomer without the side chains is almost planar (13–31°). Some anomaly of the thiophenes can be detected because of the sulfur atoms that need to be as far from each other as possible to gain the minimized energy for the molecule. The fluorinated thiophenes are not in plane with the rest of the backbone due to the repulsion effects of the sulfur and the fluorine atoms. Fluorine atom is thought to be a good choice for lowering he energy levels with no undesirable steric hindrance [2].

The monomer with the side chains, in Figure 5.12, is more planar (13–17°) than the monomer with simplified side chains, in Figure 5.13. Otherwise, the orientation of the thiophene units are alike. The side chains have an optimal geometry of a zigzag. As for the decyl side chains, they are oriented approximately parallel to the backbone. The side chains of the thiophenes are oriented on different sides of the backbone. The ester groups induce intra- and interchain nonbonding interactions that help forming a good polymer:SMA blend morphology that improves PCE [2].

Dimer 1, in Figure 5.14, is constructed in the principal of head-to-tail. In the optimized geometry, the other CRU has turned about 160 degrees vertically with respect to the first CRU according to the PES-scan. Dimer 1 is also almost planar (12–36°). The fluorinated thiophenes of each CRU are parallel, and their methyl side chains point in the same direction. The first two ester groups and their methyl side chains are located on the same side of the backbone and the last two on the other side of the backbone.

The periodical model, in Figure 5.18, was constructed to form a head-to-tail configuration. The polymeric structure of PDTB-EF-T is almost planar (21–25°), and it has a zigzag pattern. The polymer is not curved, as are not the oligomers of PDTB-EF-T. The backbone curvature of a polymer affects the solubility and charge-carrier mobility [47]. A more curved polymers are known to be more soluble but have smaller charge-carrier mobilities and polymer chain packing ability [47]. According to the article [2] a thiophene unit was set between two DTBDT-EF units to avoid the distortion of the backbone, when the new polymer PDTB-EF-T was constructed. The computational results proved that straightening the backbone by twisting the thiophene during the construction of the periodical model, the geometry of the molecule became more favorable because of the improved planarity.

The trimer, in Figure 5.20, was constructed by taking three CRUs from the periodic model, adding hydrogens, and optimizing the geometry. The planarity of the trimer is moderate (11–31°), and the biggest angles occur in the chain ends (17°, 31°). The trimer is not curved, and it has a zigzag-pattern. The ester side chains of each CRU are on the same side of the backbone plane, and the fluorinated thiophenes of each CRU are coplanar and their methyl side chains point to the same direction as in the case of dimer 1.

The structures of the simplified monomer, dimer 1, dimer2, dimer 3, trimer, and periodical model do not include the truthful side chains. The side chains were simplified by methyl groups, which affects the optimized geometry. As for the monomer, the truthful side chains prevent the twisting of the backbone and contribute to the planarity of the molecule. The same effect can be predicted for the longer oligomers and the periodical model.

5.3 Electronic structures of the optimized models

After the calculation of the optimized structure of the polymer PDTB-EF-T, its energy characteristics were studied, which includes the investigation of the electronic structure at the B3LYP/6-31G(d,p) level of theory. One-electron wave functions are also known as molecular orbitals (MO). MOs define the electronic structure of a molecule. The total energy and the levels of HOMO-1, HOMO, LUMO and LUMO+1 were calculated and shown in Table 5.1. The difference between HOMO and LUMO, the HOMO–LUMO gap, can also be seen in Table 5.1. The previous properties were also calculated for the monomers, dimer 1, dimer 2, trimer, dimer 3 cut from the periodical model, and the results are shown in Table 5.1 and illustrated in Figure 5.23. The HOMO-1, HOMO, LUMO and LUMO+1 of the periodic model are presented in Figure 5.24–5.27, respectively.

Table 5.1 *Total energies, E_{tot}, (Ha), HOMO-1, HOMO, LUMO, and LUMO+1 energies (eV), and HOMO–LUMO gaps (eV), $E_{HOMO–LUMO}$, (eV) of the compounds with side chains (+) or without side chains (-) calculated at the B3LYP/6-31G(d,p) level of theory.*

Compound	E_{tot} (Ha)	HOMO-1 (eV)	HOMO (eV)	LUMO (eV)	LUMO+1 (eV)	$E_{HOMO–LUMO}$ (eV)
Monomer (+)	-6 727.494	-7.72	-5.24	-2.25	-1.69	3.00
Monomer (-)	-5 469.331	-5.97	-5.47	-2.48	-1.82	2.99
Dimer 1 (-)	-10 937.468	-5.59	-5.39	-2.79	-2.48	2.60
Dimer 2 (-)	-10 937.446	-5.66	-5.43	-2.81	-2.48	2.62
Trimer (-)	-16 405.605	-5.52	-5.40	-2.91	-2.75	2.49
Periodic model, dimer 2 model (-)	-10 936.273	-5.79	-5.39	-3.01	-2.58	2.38
Dimer 3 cut from the periodical model (-)	-10 937.461	-5.64	-5.41	-2.82	-2.50	2.59

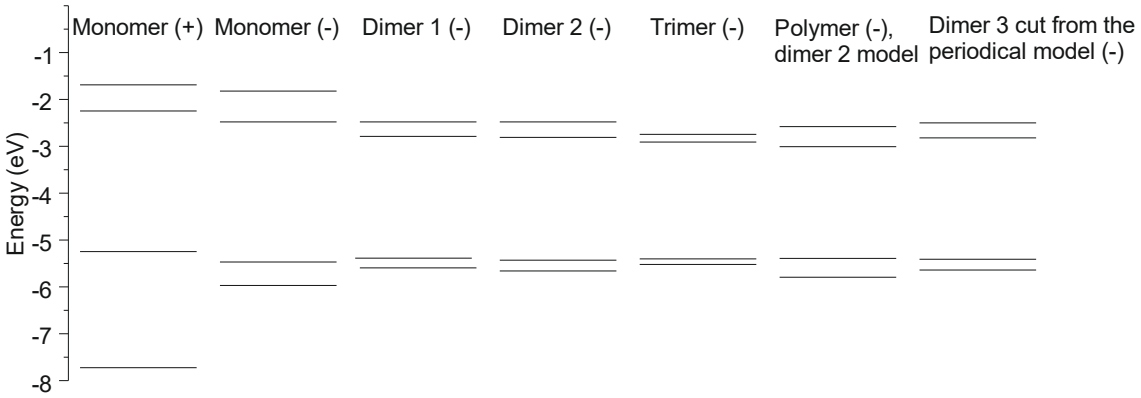

Figure 5.23 *Energies of HOMO-1 (the lowest values), HOMO (the second lowest values), LUMO (the second highest values), and LUMO+1 (the highest values) of the compounds.*

It can be seen in Table 5.1 that the side chains lower the level of HOMO-1, raise the levels of HOMO, LUMO and LUMO+1 and widen the HOMO–LUMO gap of the monomer. The truthful side chains have also a great impact on the energy characteristics of the periodic model. To point out a value, the truthful HOMO level would most probably be higher than -5.39 eV, if the side chains were included in the periodic model. Though, the behavior of the periodical model cannot predict only from the behavior of the monomer with or without the side chains.

Dimer 1, in Figure 5.14, is the structure that was constructed from the two monomer CRUs, PES-scanned and optimized. Dimer 2, in Figure 5.17, is the structure that was modified from dimer 1 by turning the dihedral angle between the CRUs. For further details, see section 5.1. Dimer 3, in Figure 5.19, is the structure that was cut from the periodical model. The periodical model was calculated from the model of dimer 2. The biggest energy difference of these dimers is between dimer 1 and dimer 2 (0.022 Ha). The

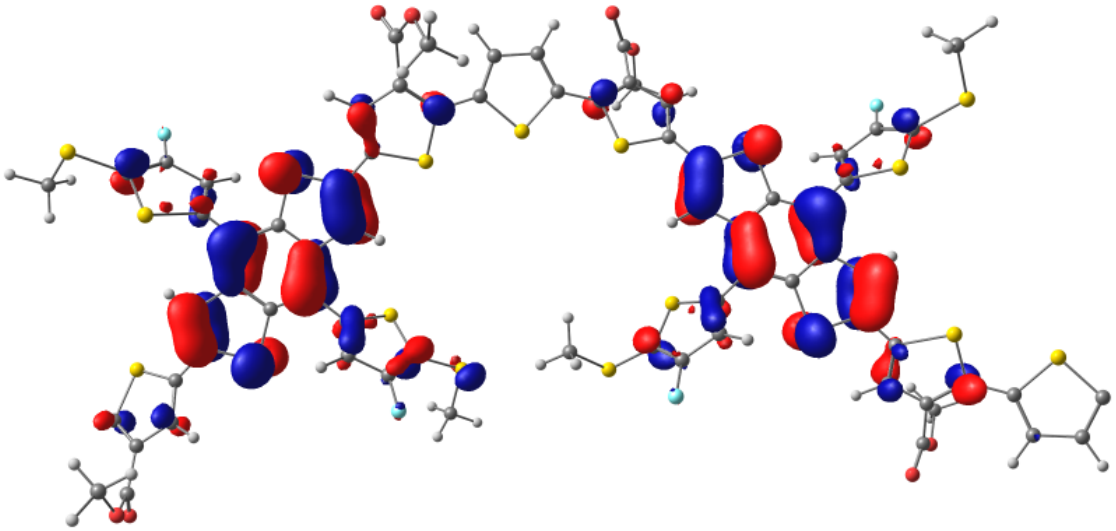

Figure 5.24 *HOMO-1 of the donor polymer PDTB-EF-T calculated at the B3LYP/6-31G(d,p) level of theory.*

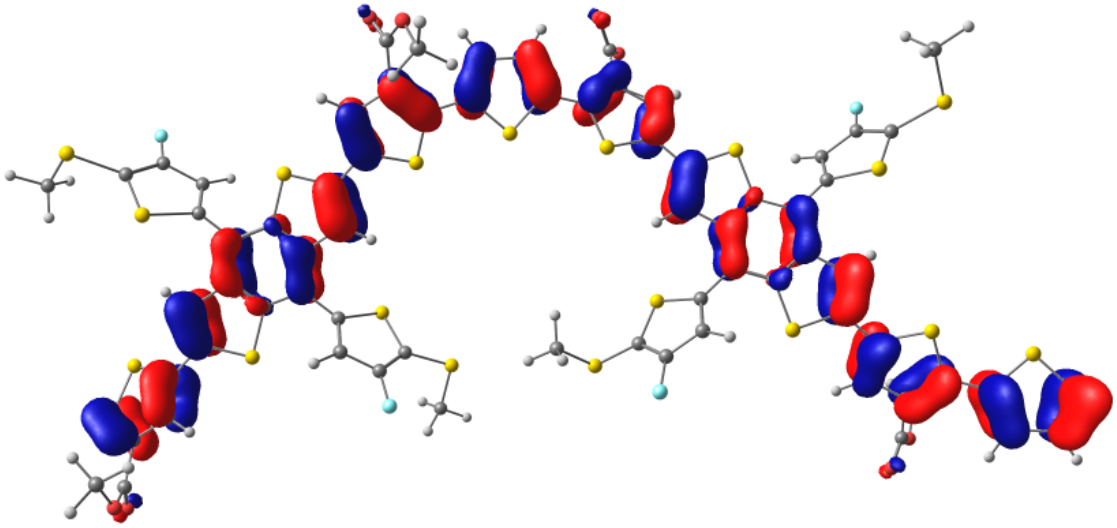

Figure 5.25 *HOMO of the donor polymer PDTB-EF-T calculated at the B3LYP/6-31G(d,p) level of theory.*

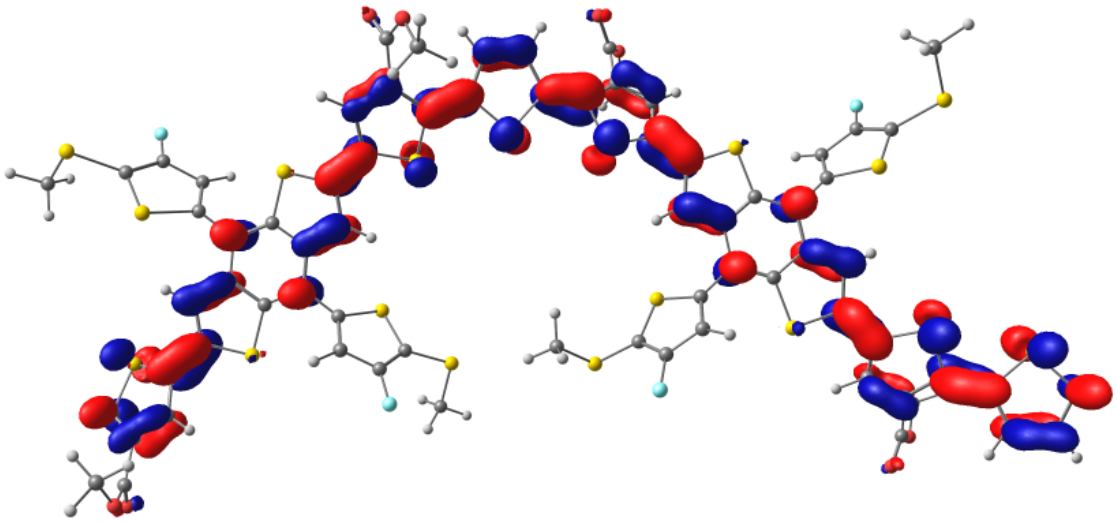

Figure 5.26 *LUMO of the donor polymer PDTB-EF-T calculated at the B3LYP/6-31G(d,p) level of theory.*

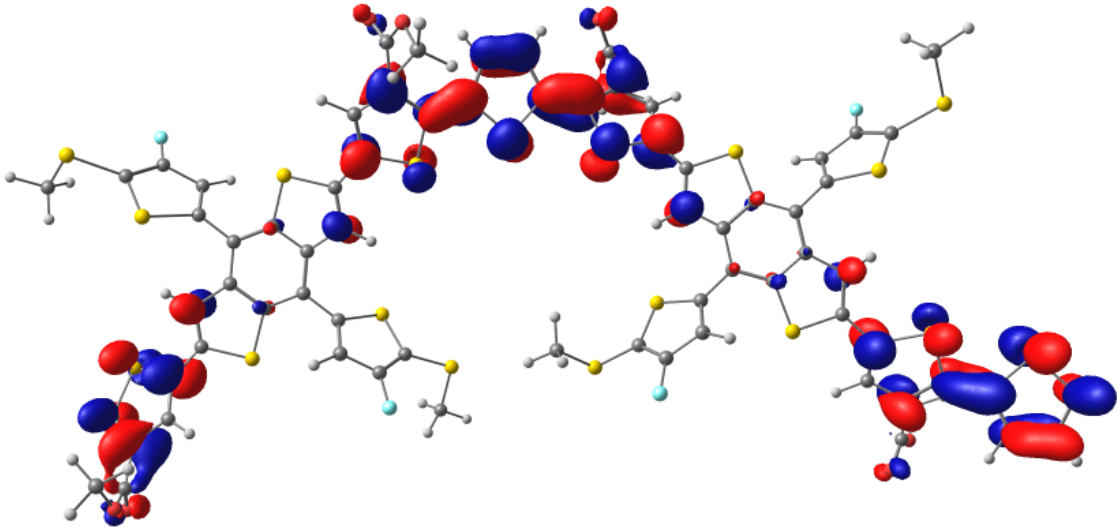

Figure 5.27 *LUMO+1 of the donor polymer PDTB-EF-T calculated at the B3LYP/6-31G(d,p) level of theory.*

energy of the periodical model is closest to that of dimer 2, because the periodical model was constructed from the model of dimer 2.

The MO levels differ only a little between the three dimers. The biggest difference of HOMO-1s is 0.07 eV, HOMOs 0.04 eV, LUMOs 0.03 eV, and LUMO+1s 0.02 eV. Moreover, the overall trend is that the HOMO-1 and HOMO levels rise and the LUMO and LUMO+1 levels lower, when the molecule length increases. In addition, the increasing backbone chain length narrows the HOMO–LUMO gap, as one would expect. The trimer does not follow the trend. It was cut from the periodical model meaning that the coordinates for the optimization of the trimer was taken after the periodical calculation. Because the periodical model was constructed from dimer 2 that is energetically more unstable

than dimer 1, the difference is also seen in the HOMO energy compared to the HOMO energy of dimer 1. Otherwise, the levels of the MOs of the trimer follow the trend.

The MOs of the periodic model presented in Table 5.1 are illustrated in Figures 5.24–5.27. The HOMO-1 wavefunction is delocalized mainly on the BDT unit. The HOMO and LUMO wavefunctions are delocalized on both CRUs in the periodic model built from dimer 2. The LUMO+1 wavefunction is delocalized mostly on the opposite places compared to HOMO-1, meaning regions other than the BDT unit and its side chains. The improved mixing and delocalization of the frontier molecular orbitals are a result of the planar backbone [48]. The HOMO and LUMO wavefunctions are delocalized over the whole backbone. Delocalization over the whole backbone indicates that the CRUs are all identical and there are no chain end effects.

The HOMO-1, HOMO, LUMO, and LUMO+1 wavefunctions for the trimer were also calculated, and they are shown in Figure 5.28–5.31, respectively. Thus, the MOs can be compared with those of the polymeric model and later with the excited states of the trimer. The MOs of the trimer and those of the periodic model in Figures 5.24–5.27 are very similar, because the trimer was cut from the periodical model. The most significant difference can be seen in the backbone chain ends. As for the trimer, the MOs do not localize in the chain ends much, because the chain ends are twisted. As mentioned in section 5.2, the angles of the thiophenes at the chain ends are 17° and 31°, which decreases the planarity of the backbone. The decrease planarity weakens the interaction between electrons and the formation of delocalized electron densities decreases. As for the polymeric model, the MOs spread throughout the whole molecule, and it has aromaticity, because the backbone is planar.

BLAs were calculated for the monomer, dimer 1, trimer, and periodic model of PDTB-EF-T. The results are shown in Table 5.2. BLAs are influenced by the length of the molecule. The BLA value decreases when the number of CRUs increase, because the delocalization of the π electrons along the backbone improves [46]. The BLA values are positive, which is due to very alternated geometries that thus are categorized as having aromatic nature [49]. By using only oligomers to define the BLA for a polymer, only the middle CRUs of the oligomer should be used for the calculations, because the backbone chain ends affect the BLA values [46].

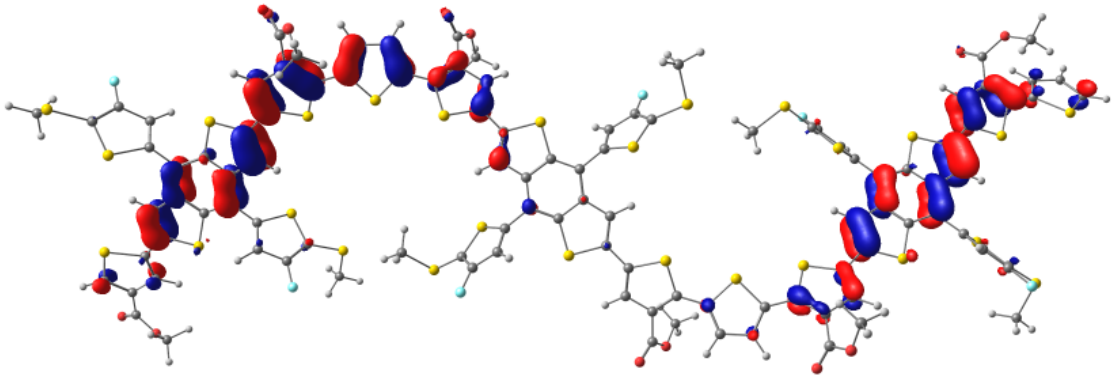

Figure 5.28 *HOMO-1 of the trimer of PDTF-EF-T.*

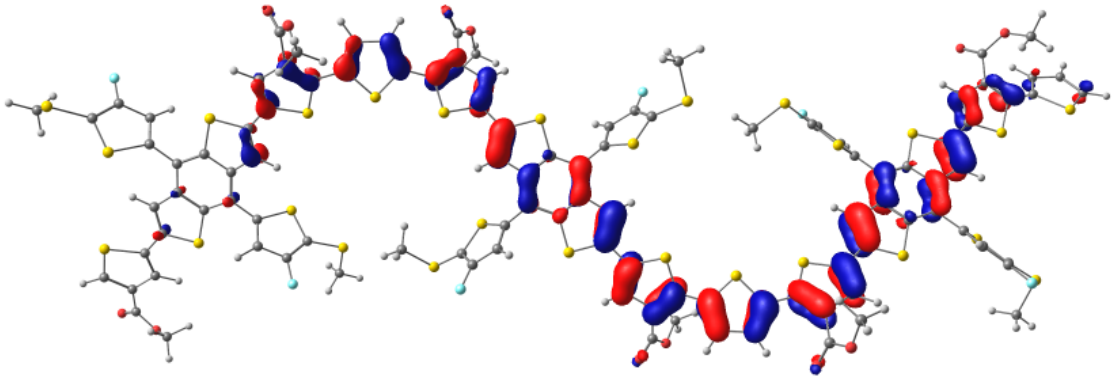

Figure 5.29 *HOMO of the trimer of PDTF-EF-T.*

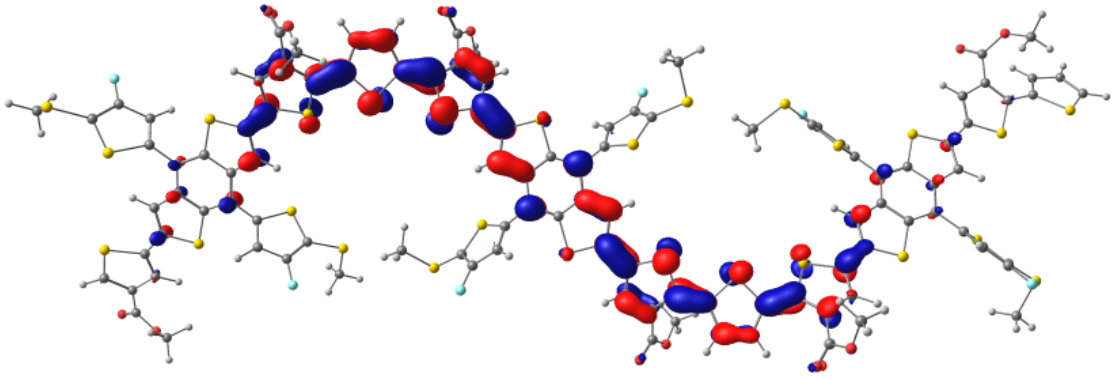

Figure 5.30 *LUMO of the trimer of PDTF-EF-T.*

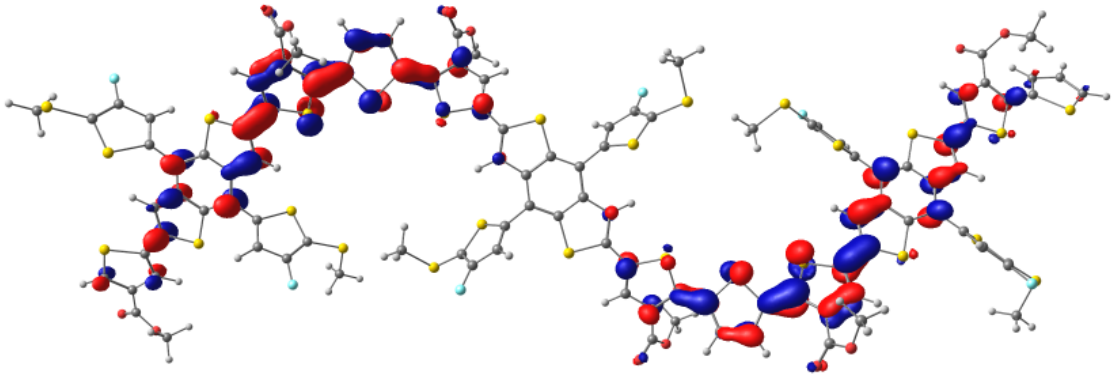

Figure 5.31 *LUMO+1 of the trimer of PDTF-EF-T.*

Table 5.2 *BLAs (Å) for the monomer, dimer 1, trimer, and periodic model of PDTB-EF-T with side chains (+) or without side chains (-).*

Molecule	**BLA (Å)**
Monomer (+)	0.0466
Monomer (-)	0.0460
Dimer 1 (-)	0.0453
Trimer (-)	0.0441
Periodic model, dimer 2 model (-)	0.0429

In order to compare the results of the theoretical calculations of this work with both the experimental results and those obtained for other polymers presented in literature, the MO levels are collected here. The results of the article [2] indicate that the HOMO level of the polymer PDTB-EF-T is about -5.5 eV and the band gap approximately 1.93 eV. The HOMO level of PDTB-EF-T computationally predicted in this work is -5.39 eV, LUMO level -3.01 eV, and the HOMO–LUMO gap 2.38 eV. The HOMO level of J71 is -5.40 eV and LUMO level -3.24 eV and the band gap 2.16 eV, which were measured by electrochemical cyclic voltammetry [16].

A few requirements for an efficient polymer donor in a PSC are a deep HOMO level and a narrow band gap [50]. The HOMO level has thus developed via the molecular design from J71 to PDTB-EF-T, and the band gap has become narrower according to the experimental results in references [2] and [16]. The theoretical calculations in this work do not predict the same result. The HOMO level of PDTB-EF-T calculated theoretically is 0.11 eV higher, and the HOMO–LUMO gap 0.45 eV wider than the band gap compared to the experimental results in reference [2]. The theoretically calculated HOMO level of PDTB-EF-T is 0.01 eV higher compared to that of the experimental result of J71 in reference [16]. In addition, the HOMO–LUMO gap of PDTB-EF-T calculated in this work is 0.22 eV wider than the band gap of J71 calculated experimentally in reference [16].

There are some differences between the calculated results of the polymer PDTB-EF-T in this thesis and the experimental results of the original article [2]. The HOMO level in the article was measured with electrochemical cyclic voltammetry. It must be kept in mind

that due to the differences between the methods, the experimental values of the article and the theoretical values of this work cannot be compared directly. [14] The DFT calculations in this work were performed for one molecule in vacuum in which the solvent was not considered. Therefore, the efficiency of only one molecule cannot be predicted. In addition, the band gap and the HOMO–LUMO gap cannot be compared directly.

It must be kept in mind that the research [2] did not calculate the properties of the monomer, the oligomers, or the whole molecule of PDTB-EF-T theoretically. Therefore, the conformation of PDTB-EF-T of the theoretical calculations in this work may differ from the truthful conformation of the polymer in the experimental measurements in reference [2]. The research did calculate the HOMO (-5.50 eV) and LUMO (-2.34 eV) levels of DTBDT-EF. The HOMO level of the monomer of PDTB-EF-T is -4.47 eV that is 0.03 eV higher than that of DTBDT-EF. The LUMO level of the monomer of PDTB-EF-T is -2.48 eV that is 0.14 eV lower than that of DTBDT-EF. The difference between DTBDT-EF and the monomer of PDTB-EF-T is that DTBDT-EF lacks one of the thiophene units, which lowers HOMO and lifts LUMO, which widens the HOMO–LUMO gap. To improve the photovoltaic performance of polymer:SMA devices, the wide band gap and the deep HOMO level of donor polymers is necessary with SMAs [2].

5.4 Calculations of the charge-carrier transport properties of the trimer

The geometry of the radical cation and the radical anion of the trimer of PDTB-EF-T were optimized at the B3LYP/6-31G(d,p) level of theory using the optimized geometry of the neutral trimer as the starting structure for the optimization to model the properties of the polymer. The section focuses on the results that are important for hole transport of the donor unit. The total energies, and HOMO- and LUMO-energies are shown in Table 5.3.

Table 5.3 *The total energies (Ha), α HOMO- (eV), and β LUMO (eV) energies of the trimer radical cation and radical anion.*

Molecule	Total energy (Ha)	α HOMO (eV)	α LUMO (eV)	β HOMO (eV)	β LUMO (eV)
Trimer radical cation	-16 405.389	-6.76	-4.58	-6.57	-6.34
Trimer radical anion	-16 405.694	-1.94	-1.64	-3.63	-1.49

The structural differences are inevitable between the ground state and cationic or anionic state. The geometry of the cationic molecule changes depending on the location where the electronic density is altered upon ionization. A cation geometry tends to have a quinoidal structure, although aromatic rings keep their aromaticity, and has increased planarity due to improved double bond character of adjacent rings. A planar structure is needed for conjugation and charge delocalization. [51] The amorphous morphology of NF acceptors sets drawbacks in charge carrier mobility, because in this case only planar

conjugated backbones and high crystallinity are helpful for charge carrier transport properties. [25]

According to Table 5.3, the total energy of the neutral trimer molecule is -16 405.605 Ha. The HOMO energy of the neutral molecule is -5.42 eV and LUMO -2.91 eV. Both HOMO and LUMO levels of the radical cation are lower than HOMO and LUMO of the neutral molecule. As for the anion, both MO levels are higher than those of the neutral molecule. The positive charge lowers, and the negative charge lifts the MO levels.

The same effects are predicted for the periodic model. The total energy of the periodic model is -10 936.273 Ha and HOMO and LUMO are -5.39 eV and -3.01 eV, respectively. The energy of the radical cation is predicted to be higher and that of the radical anion to be lower than -10 936.273 Ha. Both HOMO and LUMO levels of the radical cation of the periodic model are predicted to be lower than -5.39 eV and -3.01 eV, respectively. As for the radical anion, both HOMO and LUMO levels are predicted to be higher than those of the neutral periodic model.

The values determining hole and electron transport were also examined using equations 3.7–3.14. The energies of the different structures are shown in Table 5.4. As mentioned before, the superscript means the electronic state and the value between parentheses means the optimized geometry. 0 stands for neutral, + cation, and – anion. The results are summoned in Table 5.5.

Table 5.4 *The values (Ha) that affect charge-carrier transport properties for the trimer.*

E^0(0) (Ha)	-16 405.605	**E^0(-) (Ha)**	-16 405.602
E^+(+) (Ha)	-16 405.389	**E^+(0) (Ha)**	-16 405.386
E^-(-) (Ha)	-16 405.694	**E^-(0) (Ha)**	-16 405.691
E^0(+) (Ha)	-16 405.602		

Table 5.5 *VIP, AIP, VEA, AEA, λ_1^+, λ_2^+, λ_1^-, and λ_2^- (Ha), (eV) for the trimer.*

Energy	**(Ha)**	**(eV)**
VIP	0.219	5.96
AIP	0.216	5.88
VEA	0.085	-2.32
AEA	-0.089	-2.42
λ_1^+	0.004	0.10
λ_2^+	0.003	0.09
λ^+	0.007	0.18
λ_1^-	0.004	0.11
λ_2^-	0.004	0.10
λ^-	0.008	0.21

The Koopmans' theory, which states that the IP is about the inverse energy of HOMO and the EA is approximately the energy of LUMO, is here directional for the energy characteristics. The inverse of HOMO (5.42 eV) is ~0.5 eV smaller than VIP and LUMO, -2.91 eV, is ~0.6 eV smaller than VEA. VIP is a little higher than AIP (~0.09 eV). Thus, the VIP of the periodic model can be foreseen to be higher than 5.39 eV and the VEA to be higher than -3.01 eV. The higher ionization values are essential for an efficient hole transport and the stability of radical cations [51].

Since the hole and electron transporting at the molecular level can be represented as the electron or hole transport reactions between the neighboring atoms, the lower reorganization energy displays higher charge transport rate [45]. The reorganization energies of the trimer are in the range of 0.18 eV to 0.21 eV. The hole transport λ^+ value is less than the electron transport λ^- value resulting in a faster hole transport than electron transport of the trimer. Thus, the periodic model is assumed also to transport holes better than electrons. A better hole mobility could be gained by improving the planarity of the molecule [52]. The calculations were though performed with the trimer without the truthful side chains. The hole transport rate could be expected to increase if the planarity is increasing with the extended side chains.

A donor molecule must have great charge-carrier transport properties to move holes from the interface of a donor and an acceptor towards the anode to contribute to high PCEs [6]. A radical cation with high HOMO orbital energy, low λ^+ reorganization energy and high ionization potential transports holes efficiently [45]. Thus, the polymer PDTB-EF-T would transport holes faster through the development of the radical cation geometry.

5.5 Calculations of the excited states of the trimer

The optimized geometries of the lowest singlet and triplet excited states were calculated using TDDFT at the B3LYP/6-31(d) level by starting from the optimized geometry of the ground state of the trimer. The purpose of the calculations is to compare the geometries of the singlet and triplet excited states to the ground state geometry. The energy of the first singlet excited state and that of the triplet excited state are shown in Table 5.6. The excitation affects the MO energies of a molecule. The HOMO and LUMO energy levels of the first singlet and the first triplet states were calculated and summoned in Table 5.6. The visualizations of the orbitals are shown in Figure 5.32–5.35. The effect of the excitations is examined also with BLA values that are shown in Table 5.7.

Table 5.6 *The total energy (eV), HOMO energy (eV) and LUMO energy (eV) of the optimized geometries of the ground state and the first singlet and triplet excited states of the trimer.*

Excited state	Total energy (Ha)	HOMO (eV)	LUMO (eV)
Ground state	-16 405.605	-5.42	-2.91
Singlet	-16 405.443	-5.14	-3.18
Triplet	-16 405.473	-5.03	-3.35

The total energy of S_1 is 0.162 Ha higher than that of S_0. The HOMO level of S_1 is 0.28 eV higher and the LUMO level of S_1 is 0.27 eV lower in energy than those of S_0. The HOMO–LUMO gap of S_1 is 0.55 eV narrower in energy than that of S_0. The total energy of T_1 is 0.132 Ha higher than that of S_0. The HOMO level of T_1 is 0.39 eV higher in energy and the LUMO level of T_1 is 0.44 eV lower in energy than those of S_0. The HOMO–LUMO gap of T_1 is 0.83 eV narrower in energy than that of S_0. The dihedral angles of S_1 are 0–17°, except the angle between the two thiophenes on the most right is 29°. The dihedral angles of T_1 are 0–23°, except the angle between the two thiophenes on the most right is 30°. Compared to the dihedral angles of the S_0 geometry (11–31°) the planarity of the backbones improves little for these first excited states, which is also predicted for the periodical model.

The same effects are predicted for the periodic model. The total energy of the periodic model is -10 936.273 Ha and HOMO and LUMO are -5.39 eV and -3.01 eV, respectively, and the HOMO–LUMO gap is 2.38 eV. The energies of S_1 and T_1 of the periodical model are predicted to be higher than -10 936.273 Ha. The HOMO levels of S_1 and T_1 of the periodic model are predicted to be higher in energy than -5.39 eV and the LUMO levels of S_1 and T_1 of the periodic model are predicted to be lower in energy than -3.01 eV. The HOMO–LUMO gap of the excited states of the periodical model are predicted to be narrower in energy than 2.38 eV.

The HOMO and LUMO wavefunctions are delocalized mainly between the two CRUs of the S_1 and T_1 of the trimer. The electron densities of the HOMO and LUMO of S_1 are quite like those of S_0 and T_1 of the trimer, even though there is less electron density on the left side of S_1 of the trimer. T_1 shows to be more localized compared to S_1.

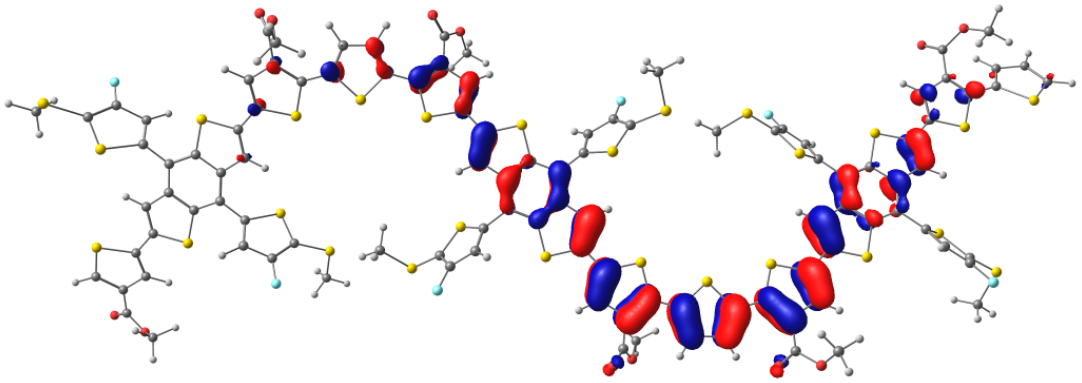

Figure 5.32 *HOMO of the lowest singlet excited state of the trimer of PDTB-EF-T.*

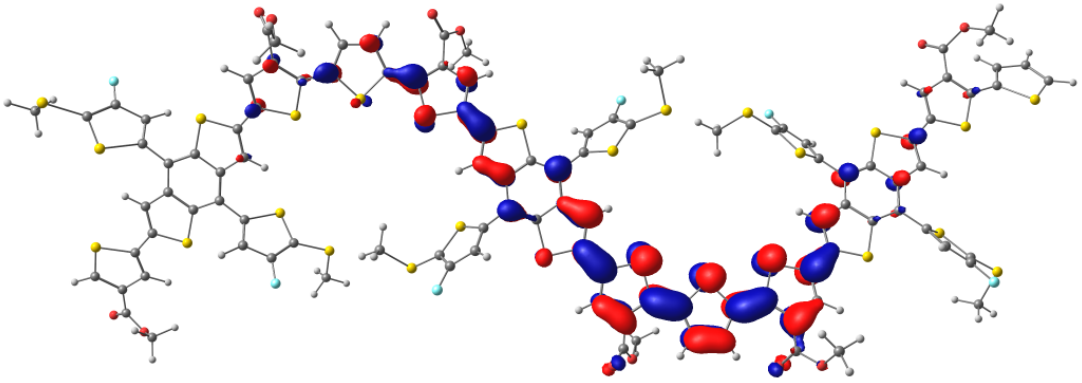

Figure 5.33 *LUMO of the lowest singlet excited state of the trimer of PDTB-EF-T.*

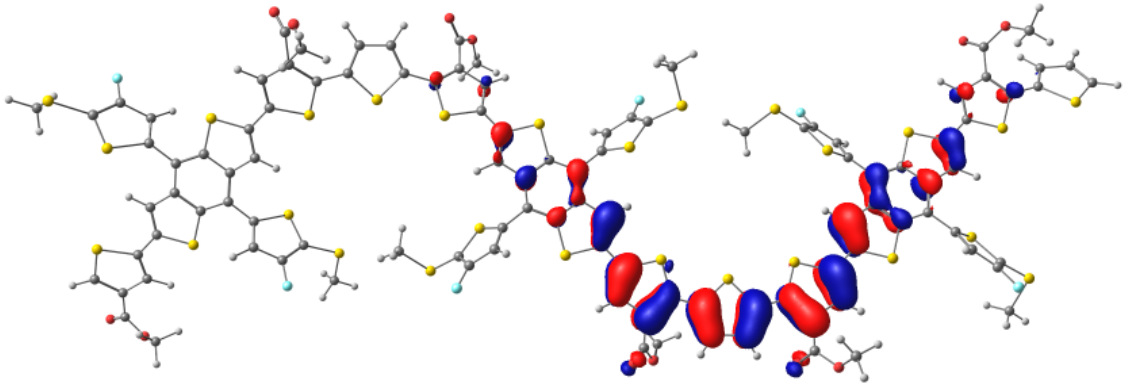

Figure 5.34 *HOMO of the lowest triplet excited state of the trimer of PDTB-EF-T.*

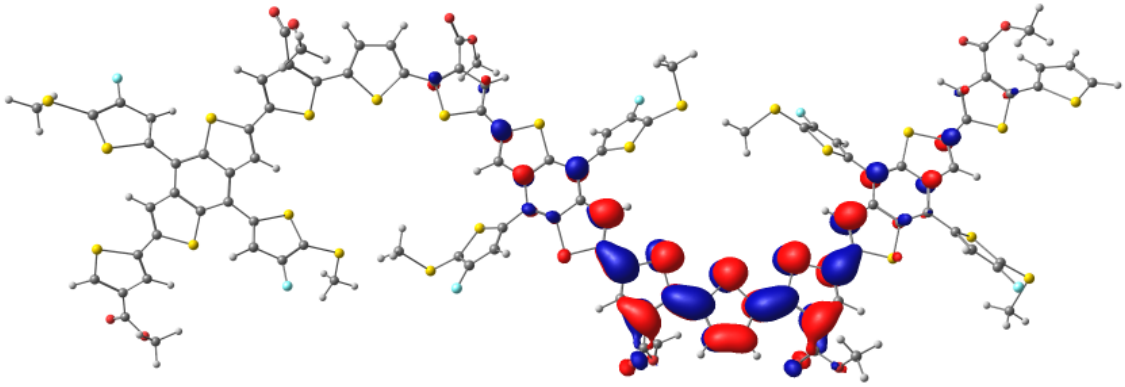

Figure 5.35 *LUMO of the lowest triplet excited state of the trimer of PDTB-EF-T.*

The MOs of S_0 of the trimer and the periodic model of PDTB-EF-T were already compared in section 5.3. The results indicated that the MOs are very similar. The most significant difference could be seen in the backbone chain ends. As for S_0 of the trimer, the MOs do not localize in the backbone chain ends much, and as for the polymeric model, the MOs spread throughout the whole molecule. The same effect is predicted for the excited states. Thus, the MOs of the excited states of the periodic model would spread more.

Table 5.7 *BLAs (Å) of S_1 and T_1 of the trimer.*

State	**BLA (Å)**
S_1	0.0226
T_1	0.0201

The BLA values of S_1 and T_1 are very close to each other according to Table 5.7. The positive BLA values mean an aromatic character of the molecule and a negative BLA value means a quinoidal character. [49] The BLA of S_1 is 0.0215 Å shorter than that of S_0 (0.0441 Å), because the excitation shortens the single bonds and lengthens the double bonds of the geometry of S_1 of the trimer [52]. The BLA of T_1 is 0.024 Å shorter than that of S_0. The BLA values indicate, that the structures of the molecules change towards a quinoid character during the excitations. A ground state geometry has an aromatic structure, whereas the excited state geometries favor more quinoid character [49]. The same effect is predicted for the periodical model. Thus, the BLA values of the S_1 and T_1 are predicted to be shorter in length than 0.0429 Å that is the BLA of S_0 of the periodical model. Moreover, the excited states of the periodical model are expected to have a quinoid character.

The vertical transition energies were also calculated using TDDFT at the B3LYP/6-31(d) level of theory for the first two singlet and the first triplet excited states, which are shown in Table 5.8. The transitions were calculated with the optimized geometry of the ground state of the trimer. The other excitations between molecular orbitals than the excitations between HOMO-1, HOMO, LUMO, and LUMO+1 were not considered for the first vertical transition of the triplet excitation in Table 5.8.

Table 5.8 *Vertical $S_0 \rightarrow S_1$ $S_0 \rightarrow S_2$ $S_0 \rightarrow T_1$ transition energies (eV) and wavelengths (λ), oscillator strengths (f), and the electronic configurations between HOMO-1, HOMO, LUMO, and LUMO+1of the trimer calculated in vacuum with TDDFT at the B3LYP/6-31G(d) level of theory using the geometry of the ground state of the trimer.*

Transition	E_{vert} (eV)	λ (nm)	f	Electronic configuration (%)
$S_0 \rightarrow S_1$	2.14	580.71	2.54	H-1→L (2.6), H-1→L+1 (7.5), H→L (84.5)
$S_0 \rightarrow S_2$	2.34	529.90	0.04	H-1→L (61.6), H→L+1 (32.6)
$S_0 \rightarrow T_1$	1.53	809.14	0	H-1→L (3.3), H-1→L+1 (13.8), H→L (54.6)

The transition energies and oscillator strengths give insight into the optical properties. As it is seen in Table 5.8, $S_0 \rightarrow S_1$ transition is ~0.2 eV smaller than $S_0 \rightarrow S_2$ transition and ~0.60 eV bigger than $S_0 \rightarrow T_1$ transition. The oscillator strengths indicate that the first vertical transition of the singlet excitation is most probable of these excitations. Although, these theoretical values can be different from those of experimental values, because these results calculated in vacuum do not consider the solvent effect.

The first vertical transition of the singlet excitation wavelength corresponds to the wavelength of visible light. The excitation is not only from HOMO to LUMO (84.5%) but also from HOMO-1 to LUMO (2.6%) and from HOMO-1 to LUMO+1 (7.5%). As for the second vertical transition of the singlet excitation, the wavelength corresponds also to the wavelength of visible light. The excitation occurs not only from HOMO-1 to LUMO (61.6%) but also from HOMO to LUMO+1 (32.6%). Finally, the first vertical transition of the triplet excitation does not correspond to the wavelength of visible light. On the other hand, it corresponds to the wavelength of a near-infrared ray. The excitation occurs mostly from HOMO to LUMO (54.6%), but also from HOMO-1 to LUMO (3.3%) and from HOMO-1 to LUMO+1 (13.8%).

The trimer of PDTB-EF-T indicates great excited state properties that are predicted also for the periodic model. Since most solar energy radiates in the frequencies of visible light and near-infrared region [29], the trimer has an overlap in this region for an absorption spectrum. The required overlap in the visible light and near-infrared region contributes to efficient harvesting of solar energy in PSCs [29].

A small energy difference between the first singlet and triplet excited state, $\Delta E_{ST,}$ is desired for efficient OPVs. As for the trimer PDTB-EF-T, ΔE_{ST}, is about 0.60 eV. For the trimer, ΔE_{ST} is approximately the same with B3LYP as literature values (~0.60 eV) for conjugated polymers. Exchange is an interaction that measures the electron–hole wavefunction overlap. Exchange energy is a measure for the electron–hole wavefunction overlap that is small for more planar and rigid polymers. By reducing the electron–hole wavefunction overlap, charge recombination becomes more improbable, which improves the photovoltaic performance. [37]

6. CONCLUSIONS

The goal of this study was to examine theoretically the photovoltaic properties of the polymer PDTB-EF-T that has yielded experimentally the highest PCE of a PSC so far, 14.2%. The properties of the polymer studied in this work were the geometry, the electronic structure, the charge-transport properties and the excited states. These characteristics are often studied for the π-conjugated systems of the donor and acceptor materials in PSCs. This work was the first theoretical study of PDTB-EF-T, in which the photovoltaic properties of the polymer were studied with QM methods. New information of the localization of the electronic density and the delocalization of the molecular orbitals of the periodical model that was illustrated with pictures, was provided. Theoretical calculations give valuable insight and guide the experimental research of the properties of a compound used in polymer solar cells.

The optimization of the polymer PDTB-EF-T was performed by first optimizing the monomer with geometry optimizations and PES-scans. Secondly, the geometry of the methyl side chained dimer 1 was optimized from the simplified monomer with geometry optimizations and a PES-scan. The periodic model was calculated from dimer 2 model that is a modified geometry of dimer 1. The trimer was constructed from the periodic model. The optimized geometry of the trimer was used to examine the charge-carrier transport properties and the excited states.

The results of the calculations followed the known theories. As the backbone chain length of the model of the polymer increases, the highest occupied molecular orbital (HOMO) and the lowest unoccupied molecular orbital (LUMO) get closer to each other, and thus, narrows the HOMO–LUMO gap. The HOMO and LUMO levels of the periodic model were calculated as -5.39 eV and -3.01 eV. The planar backbone of the polymer contributes to the chain packing efficiency and charge-carrier characteristics. According to the BLA values, the increasing backbone chain length decreases the BLA values. The planarity of the radical cation resulted proper charge-carrier transport properties, especially in the case of hole transport. As for the calculations of the excited states, the vertical transitions of the first two singlet and the first triplet excited state of the trimer of PDTB-EF-T correspond to the visible and near-infrared wavelengths.

The properties of the monomer with the truthful side chains give information, how the side chains affect the molecular geometry and the photovoltaic properties. The larger oligomers give the opportunity to examine, how the length of the donor unit affects the photovoltaic properties. A trimer is a quite short oligomer to predict the properties of a polymer accurately. The longer the oligomer, the better the properties indicate those of a polymer. Thus, based on the MO energy level and the BLA value development from the monomer to the periodic model, it is suggested to examine longer oligomers than trimer to characterize better the photovoltaic properties of the polymer PDTB-EF-T.

The thesis created a great base of the future studies that focus on the electron transport properties and the theoretical studies of the coupling of this donor molecule and the small-molecule acceptor. In the future studies, the interaction of the donor polymer PDTB-EF-T with different acceptors should also be examined. The intermutual MO levels of the donor and acceptor, the morphology between the materials and molecular packing, which affect the photovoltaic properties, could be also studied with computational methods in the future. In addition, the modifications of the conformation of the polymer PDTB-EF-T should be examined to gain even lower total energy and HOMO levels. The improvements in a deep HOMO level with a narrow band gap could be achieved with testing the effect of different electron-withdrawing side chains. Such studies would benefit the improvements in the intrinsic properties of the active materials and therefore the photovoltaic performance.

BIBLIOGRAPHY

[1] M.A. Green, K. Emery, Y. Hishikawa, W. Warta, E.D. Dunlop, Solar cell efficiency tables (version 39), Progress in Photovoltaics: Research and Applications, Vol. 20, No. 1, 2012, pp. 12–20.

[2] S. Li, L. Ye, W. Zhao, H. Yan, B. Yang, D. Liu, W. Li, H. Ade, J. Hou, A Wide Band Gap Polymer with a Deep Highest Occupied Molecular Orbital Level Enables 14.2% Efficiency in Polymer Solar Cells, Journal of the American Chemical Society, Vol. 140, No. 23, 2018, pp. 7159–7167.

[3] Frisch, M.J., Trucks, G.W., Schlegel, H.B., Scuseria, G.E., Robb, M.A., Cheeseman, J.R., Scalmani, G., Barone, V., Petersson, G.A., Nakatsuji, H., et al., Gaussian 16, Revision D.01.Gaussian Inc., Wallingford, Connecticut, 2016.

[4] Avogadro: An Open-Source Molecular Builder and Visualization Tool. Version 1.2.0. https://avogadro.cc/, accessed 25.9.2018.

[5] Chemcraft: A graphical software for visualization of quantum chemistry computations. Version 1.8. https://www.chemcraftprog.com, accessed 25.9.2018.

[6] J. Cirák, Concept of Organic Photovoltaics: Operational Principles and Materials, Acta Electrotechnica et Informatica, Vol. 13, No. 1, 2013, pp. 32–36.

[7] Polymer donor–polymer acceptor (all-polymer) solar cells, 2013, pp. 123–132.

[8] A.W. Hains, Z. Liang, M.A. Woodhouse, B.A. Gregg, Molecular Semiconductors in Organic Photovoltaic Cells, Chemical reviews, Vol. 110, No. 11, 2010, pp. 6689–6735.

[9] E.C. Yilmaz, M.K. Yesilyurt, V. G. Öner, A.N. Özakin, Operational Stability and Degradation of Organic Solar Cells, Vol. 5, No. 2, June 2017, pp. 152–160.

[10] R.P. Singh, O.S. Kushwaha, Polymer Solar Cells: An Overview, Macromolecular Symposia, Vol. 327, No. 1, 2013, pp. 128–149.

[11] H. Hoppe, N.S. Sariciftci, Organic solar cells: An overview, Journal of Materials Research, Vol. 19, No. 7, 2004, pp. 1924–1945.

[12] E.E. Havinga, W. ten Hoeve, H. Wynberg, A new class of small band gap organic polymer conductors, Polymer Bulletin, Vol. 29, No. 1, 1992, pp. 119–126.

[13] L. Dou, Y. Liu, Z. Hong, G. Li, Y. Yang, Low-Bandgap Near-IR Conjugated Polymers/Molecules for Organic Electronics, Chemical reviews, Vol. 115, No. 23, 2015, pp. 12633–12665.

[14] J. Bredas, Mind the gap! Materials Horizons, Vol. 1, No. 1, 2014, pp. 17–19.

[15] Y. Hung, J. Jiang, C. Chao, W. Su, S. Lin, Theoretical Study on the Correlation between Band Gap, Bandwidth, and Oscillator Strength in Fluorene-Based Donor–Acceptor Conjugated Copolymers, The Journal of Physical Chemistry B, Vol. 113, No. 24, 2009, pp. 8268–8277.

[16] H. Bin, L. Gao, Z. Zhang, Y. Yang, Y. Zhang, C. Zhang, S. Chen, L. Xue, C. Yang, M. Xiao, Y. Li, 11.4% Efficiency non-fullerene polymer solar cells with trialkylsilyl substituted 2D-conjugated polymer as donor, Nature Communications, Vol. 7, 2016, pp. 13651–13662.

[17] J. Liu, L. Ma, F.K. Sheong, L. Zhang, H. Hu, J. Zhang, J. Zhang, Z. Li, C. Ma, X. Han, D. Pan, H. Ade, W. Ma, H. Yan, Carboxylate substitution position influencing polymer properties and enabling non-fullerene organic solar cells with high open circuit voltage and low voltage loss, Journal of Materials Chemistry A, 2018, pp. 16874–16881.

[18] B. Carsten, J.M. Szarko, H.J. Son, W. Wang, L. Lu, F. He, B.S. Rolczynski, S.J. Lou, L.X. Chen, L. Yu, Examining the Effect of the Dipole Moment on Charge Separation in Donor–Acceptor Polymers for Organic Photovoltaic Applications, Journal of the American Chemical Society, Vol. 133, No. 50, 2011, pp. 20468–20475.

[19] F. Zhang, D. Wu, Y. Xu, X. Feng, Thiophene-based conjugated oligomers for organic solar cells, Journal of Materials Chemistry, Vol. 21, No. 44, 2011, pp. 17590–17600.

[20] Z. Li, K. Jiang, G. Yang, J.Y.L. Lai, T. Ma, J. Zhao, W. Ma, H. Yan, Donor polymer design enables efficient non-fullerene organic solar cells, Nature Communications, Vol. 7, 2016, pp. 13094–13103.

[21] R.L. Uy, S.C. Price, Y. Wei, Structure-Property Optimizations in Donor Polymers via Electronics, Substituents, and Side Chains Toward High Efficiency Solar Cells, Macromolecular Rapid Communications, Vol. 33, No. 14, 2012, pp. 1162–1177.

[22] Q. Shi, H. Fan, Y. Liu, J. Chen, L. Ma, W. Hu, Z. Shuai, Y. Li, X. Zhan, Side Chain Engineering of Copolymers Based on Bithiazole and Benzodithiophene for Enhanced Photovoltaic Performance, Macromolecules, Vol. 44, No. 11, 2011, pp. 4230–4240.

[23] Z. Zhang, J. Min, S. Zhang, J. Zhang, M. Zhang, Y. Li, Alkyl chain engineering on a dithieno[3,2-b:2',3'-d]silole-alt-dithienylthiazolo[5,4-d]thiazole copolymer toward high performance bulk heterojunction solar cells, Chemical Communications, Vol. 47, No. 33, 2011, pp. 9474–9476.

[24] F. Shen, J. Xu, X. Li, C. Zhan, Nonfullerene small-molecule acceptors with perpendicular side-chains for fullerene-free solar cells, Journal of Materials Chemistry A, Vol. 6, No. 32, 2018, pp. 15433–15455.

[25] J. Hou, O. Inganäs, R.H. Friend, F. Gao, Organic solar cells based on non-fullerene acceptors, Nature Materials, Vol. 17, 2018, pp. 119–128.

[26] Energy Harvesting Based on Polymer, in: Polymer Materials for Energy and Electronic Applications, Academic Press, photovoltaic, thermoelectric, piezoelectric, triboelectric energy harvesting, 2017, pp. 151–196.

[27] Ossila, Picture of solar cell operation, web page. Available (accessed 8.10.2018): https://www.ossila.com/pages/solar-cells-theory.

[28] Fundamentals of bulk heterojunction organic solar cells: An overview of stability/degradation issues and strategies for improvement, Bulk heterojunction organic solar cells (BHJ OSCs) Performance characteristics, Working principle, Stability, Degradation Strategies to improve, 2018, pp. 43–53.

[29] L. Lu, T. Zheng, Q. Wu, A.M. Schneider, D. Zhao, L. Yu, Recent Advances in Bulk Heterojunction Polymer Solar Cells, Chemical reviews, Vol. 115, No. 23, 2015, pp. 12666–12731.

[30] DFT theoretical investigations of π-conjugated molecules based on thienopyrazine and different acceptor moieties for organic photovoltaic cells, π-Conjugated molecules, Thienopyrazine, Organic solar cells, DFT, Low band-gap, Electronic properties (open circuit voltage), 2016, pp. S415–S425.

[31] The π-Electronic Structure of Simple Polyenes and Aromatics, web page. Limited access (accessed 12.10.2018): https://moodle2.tut.fi/pluginfile.php/522186/mod_folder/content/0/Laboratory1-PiConjugatedSytems.pdf?forcedownload=1.

[32] F. Laquai, D. Andrienko, R. Mauer, P.W.M. Blom, Charge Carrier Transport and Photogeneration in P3HT:PCBM Photovoltaic Blends, Macromolecular Rapid Communications, Vol. 36, No. 11, 2015, pp. 1001–1025.

[33] Charge-Carrier Transport Properties of Oligoacenes, web page. Limited access (accessed 12.10.2018): https://moodle2.tut.fi/pluginfile.php/522204/mod_folder/content/0/Laboratory2-ChargeCarrierTransportProperties.pdf?forcedownload=1.

[34] Color and Light in π-Conjugated systems, web page. Limited access (accessed 12.10.2018): https://moodle2.tut.fi/pluginfile.php/522217/mod_folder/content/0/Laboratory3-ColorandLightPiConjugatedSystems%20%28002%29.pdf?forcedownload=1.

[35] Oxford Dictionary, Singlet, web page. Available (accessed 14.10.2018): https://en.oxforddictionaries.com/definition/singlet.

[36] Oxford Dictionary, Triplet, web page. Available (accessed 14.10.2018): https://en.oxforddictionaries.com/definition/triplet.

[37] A. Köhler, D. Beljonne, The Singlet–Triplet Exchange Energy in Conjugated Polymers, Advanced Functional Materials, Vol. 14, No. 1, 2004, pp. 11–18.

[38] C.J. Cramer, Essentials of Computational Chemistry: Theories and Models, 2nd edition ed. John Wiley & Sons Ltd, Chichester, England, UK, 2004.

[39] E.G. Lewars, Density Functional Calculations, in: E.G. Lewars (ed.), Computational Chemistry: Introduction to the Theory and Applications of Molecular and Quantum Mechanics, Springer Netherlands, Dordrecht, 2011, pp. 445–519.

[40] V. Dragojlovic, Conformational analysis of cycloalkanes, ChemTexts, Vol. 1, No. 3, 2015, pp. 14–44.

[41] Conformational analysis of small molecules: NMR and quantum mechanics calculations, Conformational preferences, NMR, Quantum mechanical calculations, Spin–spin coupling constants, Stereo electronic interactions, 2016, pp. 73–88.

[42] B. Thompson, J. Fréchet, Polymer–Fullerene Composite Solar Cells, Angewandte Chemie International Edition, Vol. 47, No. 1, 2008, pp. 58–77.

[43] P. Kar, Electronic Parameter Responsible for Charge Transport, in: Doping in Conjugated Polymers, Scrivener Publishing, Beverly, MA, 2013, pp. 70–71.

[44] D.P. McMahon, A. Troisi, Evaluation of the External Reorganization Energy of Polyacenes, The Journal of Physical Chemistry Letters, Vol. 1, No. 6, 2010, pp. 941–946.

[45] U. Purushotham, G.N. Sastry, Conjugate acene fused buckybowls: evaluating their suitability for p-type, ambipolar and n-type air stable organic semiconductors, Physical Chemistry Chemical Physics, Vol. 15, No. 14, 2013, pp. 5039–5048.

[46] D. Jacquemin, C. Adamo, Bond Length Alternation of Conjugated Oligomers: Wave Function and DFT Benchmarks, Journal of Chemical Theory and Computation, Vol. 7, No. 2, 2011, pp. 369–376.

[47] R. Rieger, D. Beckmann, A. Mavrinskiy, M. Kastler, K. Miillen, Backbone Curvature in Polythiophenes, Chemistry of Materials, Vol. 22, No. 18, 2010, pp. 5314–5318.

[48] Donor–Acceptor Copolymers of Relevance for Organic Photovoltaics: A Theoretical Investigation of the Impact of Chemical Structure Modifications on the Electronic and Optical Properties, 2012, pp. 6405–6414.

[49] S. Suramitr, W. Meeto, P. Wolschann, S. Hannongbua, Understanding on absorption and fluorescence electronic transitions of carbazole-based conducting polymers: TD-DFT approaches, Vol. 125, No. Theor. Chem. Acc, 2009, pp. 35–44.

[50] T. Xu, L. Yu, How to design low bandgap polymers for highly efficient organic solar cells, Vol. 17, No 1, Materials today, 2014, pp. 11–15.

[51] M.E. Köse, Theoretical prediction of ionization/oxidation potentials in conjugated polymers, Theoretical Chemistry Accounts, Vol. 128, No. 2, 2011, pp. 157–164.

[52] T. Kastinen, M. Niskanen, C. Risko, O. Cramariuc, T.I. Hukka, Intrinsic Properties of Two Benzodithiophene-Based Donor–Acceptor Copolymers Used in Organic Solar Cells: A Quantum-Chemical Approach, The Journal of Physical Chemistry A, Vol. 120, No. 7, 2016, pp. 1051–1064.

APPENDIX A: THE COORDINATES OF THE MONOMER

Table A1 *The coordinates of the monomer.*

Atom	Coordinates		
C	-0.633682	-1.935293	0.755547
C	0.690651	-1.465185	0.571849
C	0.919120	-0.108735	0.196154
C	-0.108465	0.821136	0.003266
C	-1.432575	0.351894	0.189070
C	-2.661323	1.063559	-0.011371
C	-1.661181	-1.004685	0.562437
C	-3.782981	0.311886	0.207273
H	-2.700849	2.095706	-0.335607
S	-3.385448	-1.344228	0.684538
C	-5.170811	0.711562	0.096282
S	2.642935	0.231801	0.072779
C	3.041396	-1.424086	0.552314
C	1.919287	-2.176132	0.772211
H	1.959717	-3.208216	1.096504
C	-6.294823	-0.077986	0.045395
C	-7.506329	0.666858	-0.069484
C	-7.294216	2.024197	-0.105426
S	-5.619091	2.413664	0.010972
H	-6.281524	-1.160624	0.072108
H	-8.037150	2.803401	-0.190720
C	5.552137	-1.039048	0.673387
C	4.426744	-1.824311	0.664026
C	6.775262	-1.757673	0.823839
H	5.541288	0.041899	0.610788
S	4.876482	-3.512775	0.809859
C	6.586216	-3.135026	0.924232
C	8.021468	-0.955543	0.937196
S	7.091272	-5.595966	2.139225
C	7.504341	-4.254886	1.075723
C	8.697734	-4.509834	0.436532
C	8.523982	-6.457639	1.697700
C	9.276206	-5.758665	0.791750
H	9.132692	-3.819568	-0.272509
H	8.729894	-7.423145	2.138365
H	10.211512	-6.125391	0.384956
C	-0.935608	-3.326878	1.129437
C	-1.709487	-3.768215	2.177685
C	-1.796434	-5.18207	2.221488
C	-1.132941	-5.851289	1.224016
S	-0.360718	-4.682427	0.173048
H	-2.169939	-3.120336	2.912851
F	-2.489634	-5.818743	3.180793
S	-0.951785	-7.587119	0.998910

H	1.401480	1.995330	-2.174001
F	1.744893	4.686196	-2.442675
C	0.952278	2.647889	-1.436054
C	1.054115	4.061352	-1.479152
C	0.191104	2.212729	-0.375670
C	0.401773	4.735399	-0.476793
S	0.273419	6.471363	-0.239164
S	-0.371740	3.569933	0.581439
C	-8.827732	0.003074	-0.145554
O	-8.984793	-1.202200	-0.120429
O	-9.839752	0.892933	-0.245306
O	8.015618	0.262437	0.914278
O	9.141649	-1.690837	1.083986
C	1.912211	6.829334	0.563039
C	2.073367	8.302525	0.975616
C	3.396779	8.435496	1.767564
C	3.513662	9.723133	2.594224
H	4.240780	8.36889	1.065982
H	3.500032	7.579501	2.447888
C	4.845902	9.838241	3.346280
H	2.685508	9.762208	3.316070
H	3.392826	10.602425	1.947501
C	4.955647	11.113700	4.186997
H	5.672640	9.803223	2.623924
H	4.973135	8.960448	3.994215
H	4.867651	12.009616	3.561924
H	5.915950	11.166849	4.709957
H	4.162946	11.160150	4.942306
C	2.024658	9.280767	-0.228750
H	1.251802	8.550728	1.663615
C	0.655845	9.921617	-0.489087
H	2.363892	8.754937	-1.130630
H	2.750501	10.085261	-0.063654
H	-0.112834	9.176135	-0.711689
H	0.703913	10.608486	-1.340648
H	0.320911	10.495563	0.382333
H	1.983780	6.179623	1.439236
H	2.695064	6.544217	-0.146704
C	-2.705279	-8.176323	0.807090
C	-3.295069	-8.195609	-0.614895
C	-3.509239	-6.773321	-1.172721
C	-4.470871	-6.684382	-2.366226
H	-2.539449	-6.343517	-1.454509
H	-3.898698	-6.134299	-0.368667
C	-4.704897	-5.243795	-2.839670
H	-5.435347	-7.135161	-2.090422
H	-4.089611	-7.275307	-3.209200
C	-5.667605	-5.147062	-4.026713
H	-3.741182	-4.792243	-3.110934
H	-5.093056	-4.646624	-2.00372

H	-5.289132	-5.704387	-4.891374
H	-5.813682	-4.108114	-4.339218
H	-6.651348	-5.558748	-3.773984
C	-2.501895	-9.094100	-1.585214
H	-4.292188	-8.650099	-0.485261
C	-2.418874	-10.570923	-1.181116
H	-1.489989	-8.684870	-1.697897
H	-2.968073	-9.031086	-2.574522
H	-1.848596	-10.719299	-0.258288
H	-1.924201	-11.158398	-1.961115
H	-3.416367	-10.999372	-1.027846
H	-3.315474	-7.573479	1.482966
H	-2.669415	-9.186639	1.223697
H	-12.027453	2.110220	0.503439
C	-11.168878	0.328428	-0.323386
C	-12.158336	1.480550	-0.385482
H	-13.833212	0.350546	0.390478
H	-14.505824	2.772387	0.366503
C	-13.610546	0.993581	-0.472501
H	-11.921349	2.108630	-1.253317
C	-14.627886	2.140159	-0.524262
H	-16.303306	1.013470	0.247514
H	-13.731778	0.360326	-1.362469
H	-16.978211	3.436604	0.237849
C	-16.082388	1.662517	-0.611817
H	-14.404078	2.784679	-1.386000
C	-17.100997	2.808126	-0.655764
H	-18.776519	1.679966	0.113859
H	-16.204631	1.033298	-1.504908
H	-19.452728	4.103678	0.112488
C	-18.556184	2.332090	-0.743411
H	-16.879469	3.457926	-1.514427
C	-19.575282	3.477195	-0.782771
H	-21.249996	2.349495	-0.014328
H	-18.679577	1.705692	-1.638447
C	-21.030814	3.002064	-0.870435
H	-21.967600	4.774231	-0.008652
H	-19.355758	4.130116	-1.639806
C	-22.041820	4.151914	-0.907757
H	-21.153663	2.377314	-1.765635
H	-23.069824	3.780436	-0.970339
H	-21.870415	4.802485	-1.772954
H	-11.229867	-0.311854	-1.209973
H	-11.335593	-0.307695	0.552180
H	19.151015	3.098155	-5.309665
H	19.918678	4.480302	-4.517303
H	19.010544	2.908138	-2.791924
C	18.962328	3.970830	-4.674031
C	18.320812	3.559915	-3.345382
H	17.120543	1.951446	-4.146847

H	18.311361	4.651295	-5.234717
H	17.018276	1.773573	-1.63883
C	16.976779	2.841617	-3.517600
H	18.177005	4.449850	-2.717585
C	16.327565	2.426049	-2.192013
H	15.125078	0.818686	-2.994387
H	16.286519	3.493936	-4.071633
H	15.024959	0.638313	-0.487221
C	14.983105	1.708820	-2.364955
H	16.185062	3.316540	-1.563204
C	14.334818	1.292613	-1.038899
H	13.128984	-0.311566	-1.843849
H	14.292065	2.361631	-2.917005
H	13.032438	-0.497803	0.661247
C	12.989363	0.577887	-1.213233
H	14.193553	2.182403	-0.409043
C	12.342900	0.160590	0.113640
H	11.122615	-1.440780	-0.693275
H	12.297742	1.232567	-1.761493
C	10.993582	-0.546584	-0.069835
H	12.204715	1.049758	0.744234
C	10.376931	-0.955217	1.263432
H	10.294010	0.115161	-0.591822
H	10.178334	-0.079795	1.886648
H	11.025503	-1.647946	1.805989

APPENDIX B: SEQUENCE NUMBERS LABELLED ON THE ATOMS OF THE MONOMER

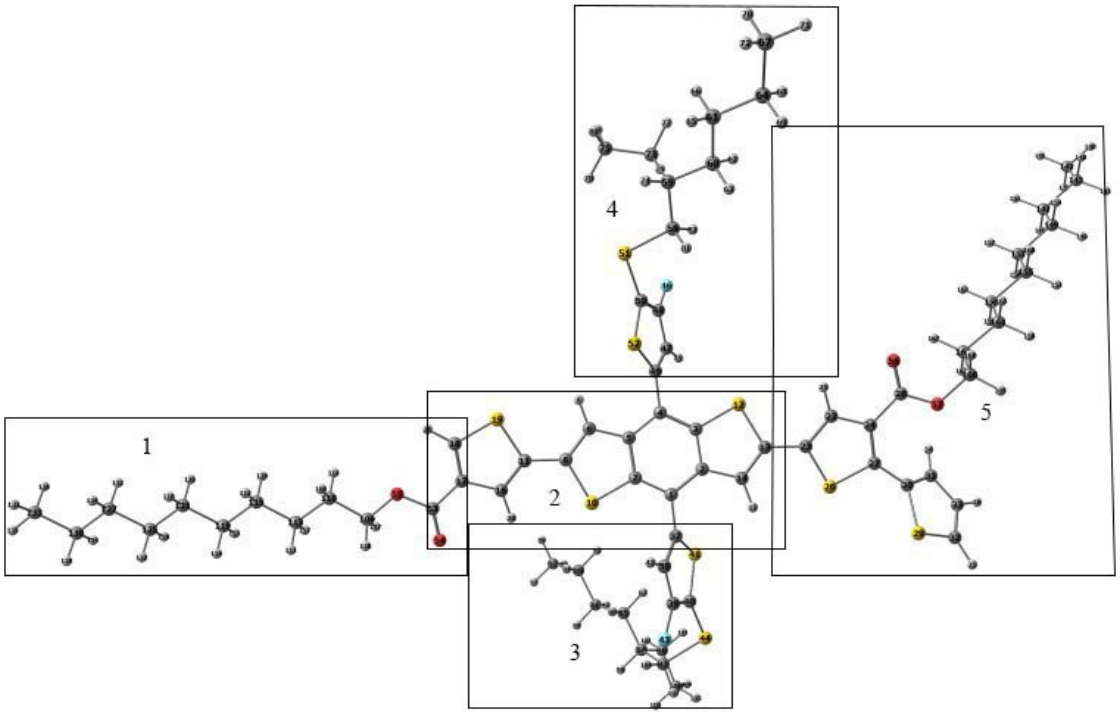

Figure B1 *Numeration of the parts of the monomer.*

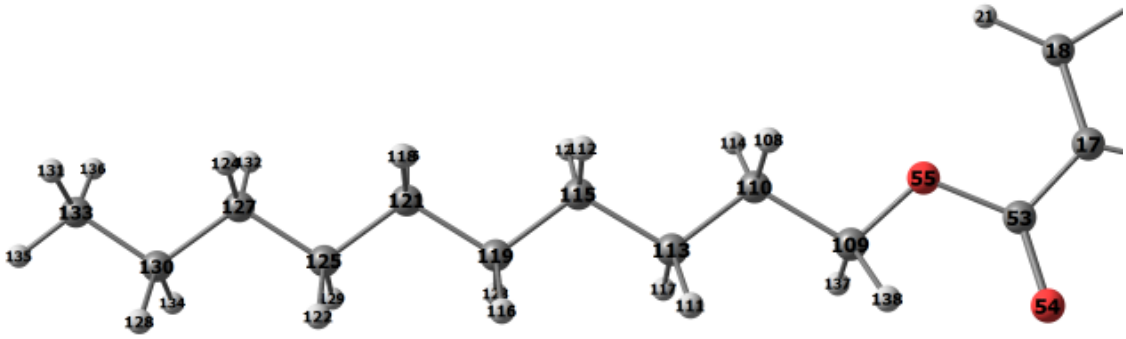

Figure B2 *Sequence numbers labelled on atoms in part 1.*

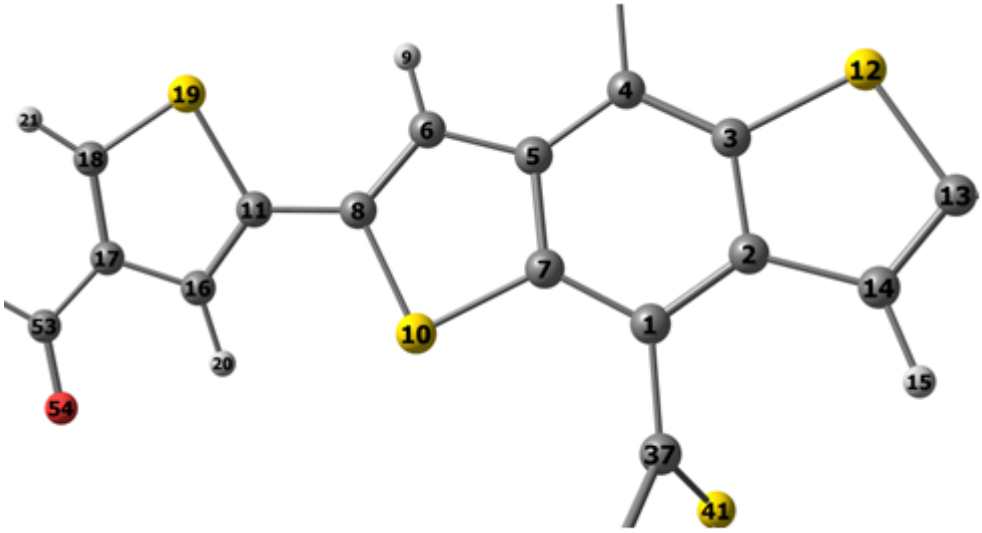

Figure B3 *Sequence numbers labelled on atoms in part 2.*

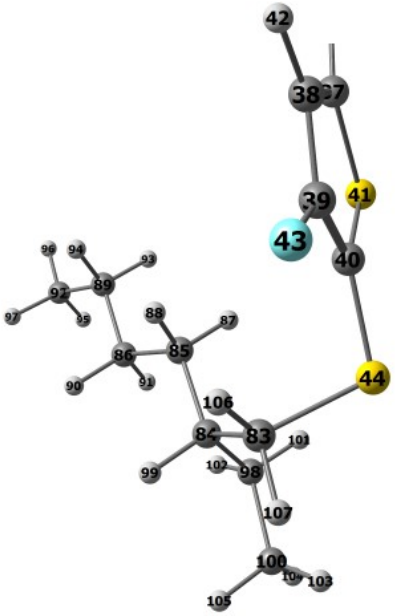

Figure B4 *Sequence numbers labelled on atoms in part 3.*

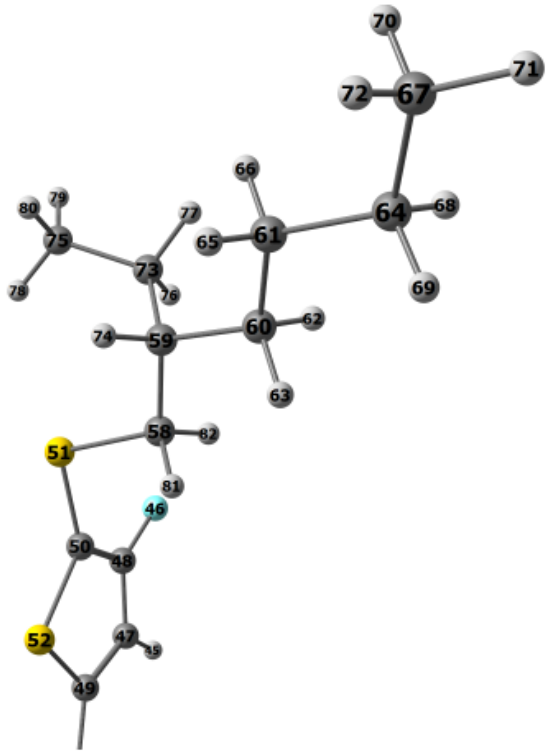

Figure B5 *Sequence numbers labelled on atoms in part 4.*

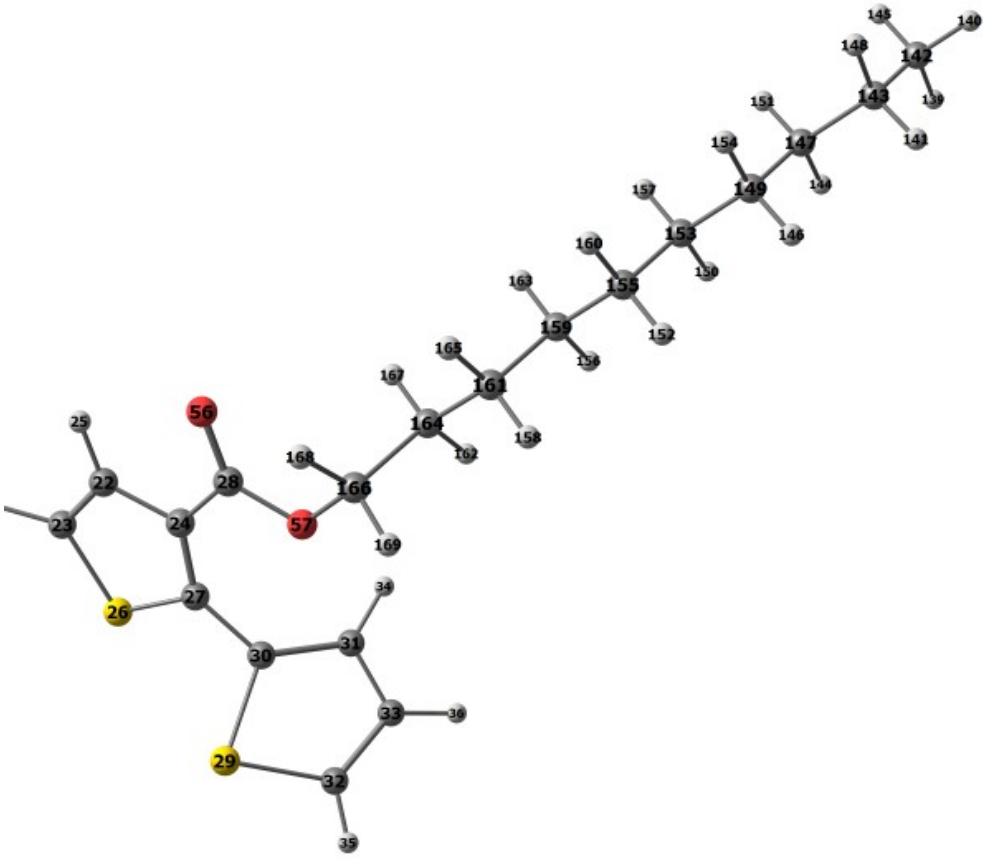

Figure B6 *Sequence numbers labelled on atoms in part 5.*

APPENDIX C: THE BOND LENGTHS OF THE MONOMER

Table C1 *The bond lengths of the monomer.*

Bond	Length (Å)	Bond	Length (Å)
R(1-2)	1.417	R(58-82)	1.094
R(2-3)	1.426	R(44-83)	1.860
R(3-4)	1.399	R(83-84)	1.540
R(4-5)	1.417	R(84-85)	1.543
R(5-6)	1.434	R(85-86)	1.535
R(1-7)	1.400	R(85-87)	1.098
R(5-7)	1.425	R(85-88)	1.098
R(6-8)	1.368	R(86-89)	1.534
R(6-9)	1.083	R(86-90)	1.100
R(7-10)	1.762	R(86-91)	1.098
R(8-10)	1.769	R(89-92)	1.531
R(8-11)	1.448	R(89-93)	1.098
R(3-12)	1.761	R(89-94)	1.098
R(12-13)	1.769	R(92-95)	1.096
R(2-14)	1.434	R(92-96)	1.095
R(13-14)	1.369	R(92-97)	1.096
R(14-15)	1.083	R(84-98)	1.542
R(11-16)	1.375	R(84-99)	1.103
R(16-17)	1.427	R(98-100)	1.533
R(17-18)	1.374	R(98-101)	1.097
R(18-19)	1.724	R(98-102)	1.095
R(11-19)	1.762	R(100-103)	1.095
R(16-20)	1.083	R(100-104)	1.095
R(18-21)	1.080	R(100-105)	1.096
R(13-23)	1.446	R(83-106)	1.092
R(22-23)	1.372	R(83-107)	1.093
R(22-24)	1.427	R(55-109)	1.446
R(22-25)	1.083	R(109-110)	1.520
R(23-26)	1.753	R(108-110)	1.097
R(26-27)	1.755	R(111-113)	1.099
R(24-27)	1.394	R(110-113)	1.534
R(24-28)	1.486	R(110-114)	1.097
R(29-30)	1.761	R(113-115)	1.534
R(27-30)	1.456	R(112-115)	1.099
R(30-31)	1.378	R(113-117)	1.099
R(29-32)	1.729	R(116-119)	1.099
R(31-33)	1.421	R(115-119)	1.533
R(32-33)	1.369	R(115-120)	1.099
R(31-34)	1.081	R(119-121)	1.534
R(32-35)	1.081	R(118-121)	1.099
R(33-36)	1.084	R(119-123)	1.099
R(1-37)	1.472	R(122-125)	1.099
R(37-38)	1.376	R(121-125)	1.534
R(38-39)	1.417	R(121-126)	1.099

R(39-40)	1.372	R(125-127)	1.533
R(40-41)	1.751	R(124-127)	1.100
R(37-41)	1.756	R(125-129)	1.099
R(38-42)	1.083	R(128-130)	1.099
R(39-43)	1.344	R(127-130)	1.534
R(40-44)	1.760	R(127-132)	1.100
R(45-47)	1.083	R(130-133)	1.532
R(47-48)	1.418	R(131-133)	1.096
R(46-48)	1.340	R(130-134)	1.099
R(47-49)	1.376	R(133-135)	1.095
R(4-49)	1.473	R(133-136)	1.096
R(48-50)	1.373	R(109-137)	1.095
R(50-51)	1.757	R(109-138)	1.095
R(49-52)	1.754	R(139-142)	1.096
R(50-52)	1.754	R(140-142)	1.095
R(17-53)	1.481	R(142-143)	1.532
R(53-54)	1.216	R(141-143)	1.099
R(53-55)	1.351	R(142-145)	1.096
R(28-56)	1.218	R(144-147)	1.100
R(28-57)	1.348	R(143-147)	1.534
R(51-58)	1.859	R(143-148)	1.099
R(58-59)	1.538	R(147-149)	1.533
R(59-60)	1.548	R(146-149)	1.099
R(60-61)	1.535	R(147-151)	1.100
R(60-62)	1.100	R(150-153)	1.099
R(60-63)	1.098	R(149-153)	1.534
R(61-64)	1.534	R(149-154)	1.099
R(61-65)	1.099	R(153-155)	1.534
R(61-66)	1.098	R(152-155)	1.099
R(64-67)	1.532	R(153-157)	1.099
R(64-68)	1.098	R(156-159)	1.099
R(64-69)	1.098	R(155-159)	1.533
R(67-70)	1.096	R(155-160)	1.099
R(67-71)	1.095	R(159-161)	1.534
R(67-72)	1.096	R(158-161)	1.099
R(59-73)	1.552	R(159-163)	1.099
R(59-74)	1.100	R(161-164)	1.534
R(73-75)	1.534	R(162-164)	1.098
R(73-76)	1.098	R(161-165)	1.099
R(73-77)	1.096	R(164-166)	1.525
R(75-78)	1.094	R(57-166)	1.449
R(75-79)	1.095	R(164-167)	1.095
R(75-80)	1.096	R(166-168)	1.093
R(58-81)	1.093	R(166-169)	1.093

APPENDIX D: THE BOND ANGLES OF THE MONOMER

Table D1 *The bond angles of the monomer.*

Bond	Angle (°)	Bond	Angle (°)
A(1-2-3)	120.0	A(84-83-107)	110.7
A(2-1-7)	116.6	A(84-85-86)	114.9
A(1-2-14)	128.2	A(84-85-87)	109.3
A(2-1-37)	122.6	A(84-85-88)	108.7
A(2-3-4)	123.4	A(85-84-98)	112.4
A(2-3-12)	111.0	A(85-84-99)	107.3
A(3-2-14)	111.8	A(86-85-87)	109.3
A(3-4-5)	116.6	A(86-85-88)	108.3
A(4-3-12)	125.5	A(85-86-89)	112.9
A(3-4-49)	120.9	A(85-86-90)	109.3
A(4-5-6)	128.2	A(85-86-91)	110.4
A(4-5-7)	120.0	A(87-85-88)	105.9
A(5-4-49)	122.5	A(89-86-90)	109.2
A(6-5-7)	111.8	A(89-86-91)	108.7
A(5-6-8)	114.1	A(86-89-92)	113.2
A(5-6-9)	123.1	A(86-89-93)	109.2
A(1-7-5)	123.4	A(86-89-94)	109.2
A(1-7-10)	125.5	A(90-86-91)	106.1
A(7-1-37)	120.9	A(92-89-93)	109.5
A(5-7-10)	111.0	A(92-89-94)	109.5
A(8-6-9)	122.8	A(89-92-95)	111.2
A(6-8-10)	111.9	A(89-92-96)	111.4
A(6-8-11)	128.4	A(89-92-97)	111.2
A(7-10-8)	91.2	A(93-89-94)	105.9
A(10-8-11)	119.6	A(95-92-96)	107.7
A(8-11-16)	128.9	A(95-92-97)	107.5
A(8-11-19)	120.9	A(96-92-97)	107.6
A(3-12-13)	91.2	A(98-84-99)	107.4
A(12-13-14)	111.9	A(84-98-100)	115.0
A(12-13-23)	119.7	A(84-98-101)	108.8
A(2-14-13)	114.1	A(84-98-102)	108.4
A(2-14-15)	123.1	A(100-98-101)	109.7
A(13-14-15)	122.8	A(100-98-102)	108.4
A(14-13-23)	128.4	A(98-100-103)	112.4
A(11-16-17)	113.4	A(98-100-104)	110.7
A(16-11-19)	110.2	A(98-100-105)	111.3
A(11-16-20)	124.3	A(101-98-102)	106.2
A(16-17-18)	112.7	A(103-100-104)	107.0
A(17-16-20)	122.3	A(103-100-105)	107.6
A(16-17-53)	121.9	A(104-100-105)	107.5
A(17-18-19)	111.8	A(106-83-107)	107.0

A(17-18-21)	127.5	A(55-109-110)	107.7
A(18-17-53)	125.4	A(55-109-137)	108.8
A(18-19-11)	91.8	A(55-109-138)	108.9
A(19-18-21)	120.7	A(109-110-108)	108.9
A(13-23-22)	128.9	A(109-110-113)	112.2
A(13-23-26)	121.2	A(109-110-114)	109.0
A(23-22-24)	114.6	A(110-109-137)	111.9
A(23-22-25)	124.2	A(110-109-138)	112.0
A(22-23-26)	109.9	A(108-110-113)	109.9
A(24-22-25)	121.2	A(108-110-114)	106.7
A(22-24-27)	112.9	A(111-113-110)	109.4
A(22-24-28)	117.1	A(111-113-115)	109.2
A(23-26-27)	92.8	A(111-113-117)	106.0
A(26-27-24)	109.9	A(113-110-114)	110.0
A(26-27-30)	117.1	A(110-113-115)	113.1
A(27-24-28)	129.9	A(110-113-117)	109.5
A(24-27-30)	133.0	A(113-115-112)	109.2
A(24-28-56)	122.3	A(115-113-117)	109.3
A(24-28-57)	114.2	A(113-115-119)	113.5
A(29-30-27)	120.0	A(113-115-120)	109.3
A(29-30-31)	110.0	A(112-115-119)	109.3
A(30-29-32)	91.8	A(112-115-120)	106.0
A(27-30-31)	129.8	A(116-119-115)	109.3
A(30-31-33)	113.5	A(116-119-121)	109.3
A(30-31-34)	122.3	A(116-119-123)	105.9
A(29-32-33)	111.7	A(119-115-120)	109.3
A(29-32-35)	119.9	A(115-119-121)	113.5
A(31-33-32)	113.0	A(115-119-123)	109.3
A(33-31-34)	124.1	A(119-121-118)	109.2
A(31-33-36)	123.7	A(121-119-123)	109.3
A(33-32-35)	128.4	A(119-121-125)	113.6
A(32-33-36)	123.3	A(119-121-126)	109.3
A(1-37-38)	127.7	A(118-121-125)	109.3
A(1-37-41)	121.6	A(118-121-126)	105.9
A(37-38-39)	112.2	A(122-125-121)	109.3
A(38-37-41)	110.6	A(122-125-127)	109.3
A(37-38-42)	124.4	A(122-125-129)	105.9
A(38-39-40)	115.7	A(125-121-126)	109.3
A(39-38-42)	123.4	A(121-125-127)	113.6
A(38-39-43)	121.8	A(121-125-129)	109.3
A(39-40-41)	108.9	A(125-127-124)	109.3
A(40-39-43)	122.5	A(127-125-129)	109.3
A(39-40-44)	128.6	A(125-127-130)	113.6
A(40-41-37)	92.5	A(125-127-132)	109.3
A(41-40-44)	122.4	A(124-127-130)	109.2
A(40-44-83)	103.2	A(124-127-132)	105.9

A(45-47-48)	123.4	A(128-130-127)	109.2
A(45-47-49)	124.3	A(128-130-133)	109.5
A(47-48-46)	121.6	A(128-130-134)	106.0
A(48-47-49)	112.2	A(130-127-132)	109.2
A(47-48-50)	115.7	A(127-130-133)	113.3
A(46-48-50)	122.7	A(127-130-134)	109.2
A(47-49-4)	127.6	A(130-133-131)	111.2
A(47-49-52)	110.7	A(133-130-134)	109.5
A(4-49-52)	121.7	A(130-133-135)	111.5
A(48-50-51)	128.2	A(130-133-136)	111.2
A(48-50-52)	108.9	A(131-133-135)	107.6
A(51-50-52)	122.9	A(131-133-136)	107.5
A(50-51-58)	100.6	A(135-133-136)	107.6
A(49-52-50)	92.5	A(137-109-138)	107.4
A(17-53-54)	124.0	A(139-142-140)	107.6
A(17-53-55)	112.1	A(139-142-143)	111.2
A(54-53-55)	123.9	A(139-142-145)	107.5
A(53-55-109)	115.8	A(140-142-143)	111.5
A(56-28-57)	123.5	A(140-142-145)	107.6
A(28-57-166)	116.4	A(142-143-141)	109.5
A(51-58-59)	113.1	A(143-142-145)	111.2
A(51-58-81)	106.8	A(142-143-147)	113.3
A(51-58-82)	107.5	A(142-143-148)	109.5
A(58-59-60)	108.0	A(141-143-147)	109.2
A(58-59-73)	113.1	A(141-143-148)	106.0
A(58-59-74)	107.8	A(144-147-143)	109.2
A(59-58-81)	110.3	A(144-147-149)	109.3
A(59-58-82)	110.4	A(144-147-151)	105.9
A(59-60-61)	114.4	A(147-143-148)	109.2
A(59-60-62)	108.9	A(143-147-149)	113.6
A(59-60-63)	109.3	A(143-147-151)	109.2
A(60-59-73)	111.7	A(147-149-146)	109.3
A(60-59-74)	107.4	A(149-147-151)	109.3
A(61-60-62)	109.6	A(147-149-153)	113.6
A(61-60-63)	108.2	A(147-149-154)	109.3
A(60-61-64)	113.2	A(146-149-153)	109.3
A(60-61-65)	109.0	A(146-149-154)	105.9
A(60-61-66)	110.3	A(150-153-149)	109.3
A(62-60-63)	106.0	A(150-153-155)	109.3
A(64-61-65)	109.2	A(150-153-157)	105.9
A(64-61-66)	108.9	A(153-149-154)	109.2
A(61-64-67)	113.2	A(149-153-155)	113.6
A(61-64-68)	109.2	A(149-153-157)	109.3
A(61-64-69)	109.3	A(153-155-152)	109.3
A(65-61-66)	106.0	A(155-153-157)	109.2
A(67-64-68)	109.5	A(153-155-159)	113.5

A(67-64-69)	109.5	A(153-155-160)	109.3
A(64-67-70)	111.2	A(152-155-159)	109.3
A(64-67-71)	111.4	A(152-155-160)	106.0
A(64-67-72)	111.2	A(156-159-155)	109.3
A(68-64-69)	106.0	A(156-159-161)	109.2
A(70-67-71)	107.6	A(156-159-163)	106.0
A(70-67-72)	107.5	A(159-155-160)	109.2
A(71-67-72)	107.6	A(155-159-161)	113.5
A(73-59-74)	108.6	A(155-159-163)	109.3
A(59-73-75)	115.0	A(159-161-158)	109.2
A(59-73-76)	109.0	A(161-159-163)	109.2
A(59-73-77)	109.0	A(159-161-164)	113.1
A(75-73-76)	109.7	A(159-161-165)	109.2
A(75-73-77)	108.1	A(158-161-164)	109.6
A(73-75-78)	112.1	A(158-161-165)	106.1
A(73-75-79)	110.8	A(161-164-162)	109.9
A(73-75-80)	110.9	A(164-161-165)	109.3
A(76-73-77)	105.7	A(161-164-166)	112.0
A(78-75-79)	107.5	A(161-164-167)	109.9
A(78-75-80)	107.7	A(162-164-166)	109.0
A(79-75-80)	107.7	A(162-164-167)	107.3
A(81-58-82)	108.5	A(164-166-57)	111.9
A(44-83-84)	117.4	A(166-164-167)	108.7
A(44-83-106)	106.7	A(164-166-168)	110.9
A(44-83-107)	102.9	A(164-166-169)	111.3
A(83-84-85)	112.1	A(57-166-168)	108.8
A(83-84-98)	113.0	A(57-166-169)	104.2
A(83-84-99)	104.1	A(168-166-169)	109.4
A(84-83-106)	111.4		